REVIEW ARTICLE

EJN European Journal of Neuroscience FENS **WILEY**

Neuronal chemo-architecture of the entorhinal cortex: A comparative review

Asgeir Kobro-Flatmoen [iD] | **Menno P. Witter** [iD]

Kavli Institute for Systems Neuroscience, Centre for Neural Computation, Egil and Pauline Braathen and Fred Kavli Centre for Cortical Microcircuits, Faculty of Medicine and Health Sciences, Norwegian University of Science and Technology (NTNU), Trondheim, Norway

Correspondence
Menno P. Witter, Faculty of Medicine and Health Sciences, Kavli Institute for Systems Neuroscience, MTFS, NTNU, Postboks 8905, 7491 Trondheim, Norway.
Email: menno.witter@ntnu.no

Abstract

The identification of neuronal markers, that is, molecules selectively present in subsets of neurons, contributes to our understanding of brain areas and the networks within them. Specifically, recognizing the distribution of different neuronal markers facilitates the identification of borders between functionally distinct brain areas. Detailed knowledge about the localization and physiological significance of neuronal markers may also provide clues to generate new hypotheses concerning aspects of normal and abnormal brain functioning. Here, we provide a comprehensive review on the distribution within the entorhinal cortex of neuronal markers and the morphology of the neurons they reveal. Emphasis is on the comparative distribution of several markers, with a focus on, but not restricted to rodent, monkey and human data, allowing to infer connectional features, across species, associated with these markers, based on what is revealed by mainly rodent data. The overall conclusion from this review is that there is an emerging pattern in the distribution of neuronal markers in the entorhinal cortex when aligning data along a comparable coordinate system in various species.

KEYWORDS

immunohistochemical markers, laminar specificity, neuroanatomy, neuron specificity, parahippocampal

1 | INTRODUCTION

The entorhinal cortex (EC) in the rodent has been the subject of increased investigations for over a decade, boosted by the first description of spatially modulated neurons in 2004 in its medial subdivision (Fyhn, Molden, Witter, Moser, & Moser, 2004). This increased attention resulted in the descriptions of several additional functional cell types, including cells coding for directionality, borders and combinations of these features, most of which have been allocated to the population of principal neurons (Rowland, Roudi, Moser, & Moser, 2016). Speed cells are a likely exception to this rule, since a substantial portion apparently belongs to the class of fast-spiking interneurons (Kropff, Carmichael, Moser, & Moser, 2015). More recently, specific functional phenotypes have been described in the lateral subdivision of EC as well. These include principal neurons coding for the position of objects or presenting a kind of memory for such object–position associations (Deshmukh & Knierim, 2011; Tsao, Moser, & Moser, 2013), and neurons whose overall population firing rates encode temporal information (Tsao et al., 2018). While the exact identity of these latter neurons remains to be determined, many of them show firing characteristics of principal neurons.

A parallel increased attention emerged, aiming to identify neurons by way of basic electrophysiological properties, often in in vitro slice studies, and in some of these studies correlated chemical and/or gene expression data have been provided. For example, using immunohistochemistry, the population of layer II/III principal neurons has been subdivided into reelin expressing neurons that project to the hippocampal dentate gyrus along with CA3 and CA2, calbindin-expressing pyramidal neurons, which apparently only sparsely project to the hippocampus, and a population that does not belong to either of these categories (Ohara et al., 2016; Varga, Lee, & Soltesz, 2010). Likewise, in a recent study, neuron types in layer V were divided based on the selective expression of two transcription factors named the chicken ovalbumin upstream promoter transcription factor-interacting protein 2 (Ctip2) and the transcription factor E twenty-six (ETS) variant 1 (Etv1; Ohara et al., 2018; Surmeli et al., 2015).

In the cortex, interneurons have been mainly identified on the basis of a combination of the expression profiles of proteins including calcium binding proteins, or certain receptors, combined with morphology. In a number of instances, electrophysiological properties are available (DeFelipe et al., 2013; Markram et al., 2004). In the hippocampus, details have been substantially worked out (Harris et al., 2018; Klausberger & Somogyi, 2008), but data on EC are still limited (for reviews, see Canto, 2011; Cappaert, Van Strien, & Witter, 2015). It is important to point out that some of the chemical markers, such as the calcium binding proteins are not selectively expressed in either interneurons or principal neurons, but generally the main distribution patterns are well characterized regarding neuron types. When relevant, details are provided, and in some instances, co-localization with other markers such as vesicular glutamate receptors have been used to differentiate between interneurons and principal neurons (Wouterlood et al., 2007). Our current knowledge suggests that in EC, all main classes of interneurons described in the neocortex are present, and correlated connectional, electrophysiological and molecular/gene expression details are beginning to be added (Couey et al., 2013; Fuchs et al., 2016; Leitner et al., 2016; Nilssen et al., 2018; Pastoll, Solanka, van Rossum, & Nolan, 2013).

In order to understand the functional contributions of neurons in networks, one needs to achieve selective manipulation of the activity of identified neuron types. During the last decade, a technological explosion provided the neuroscience community with an immense potential to achieve this (Lerner, Ye, & Deisseroth, 2016; Luo, Callaway, & Svoboda, 2008; Lykken & Kentros, 2014). To take advantage of this experimental potential in EC, regarding its functions both in the healthy brain and in the diseased brain, a thorough overview of the current knowledge database is mandatory.

The latter focus, the diseased brain, brings in another important aspect, that is, how detailed is our knowledge on neuron types in the primate brain, including both the non-human and human brain. It is well accepted that the fundamental connectional diagram of EC appears phylogenetically conserved across mammalian brains (Insausti & Amaral, 2012). Thus, EC receives information from unimodal olfactory and several multimodal sensory cortical domains, as well as multiple higher order cortical areas and subcortical structures. Dense connections between EC and the hippocampal formation have been described in all species in which they have been explored, including rats (Cappaert et al., 2015; Insausti, 1993), mice (van Groen, Miettinen, & Kadish, 2003; Witter, 2012), cats (Van Groen, Van Haren, Witter, & Groenewegen, 1986; Witter & Groenewegen, 1984), bats (Kleven, Gatome, Las, Ulanovsky, & Witter, 2014), monkeys (Insausti, 1993; Insausti & Amaral, 2008; Witter & Amaral, 1991) and recently also in humans (Zeineh et al., 2017). This highly conserved connectional scaffold not only allows for interaction between these structures, but also provides the main gateway through which information can be exchanged between the hippocampal formation and the rest of the cortex. This ability of multiple cortical regions to interact both with EC, and through it, the hippocampal formation, undoubtedly enables crucial aspects of conscious memory. This is exemplified by the impairments of conscious memory associated with damage to EC, such as in temporal lobe epilepsy (Schwarcz & Witter, 2002) and Alzheimer's disease (Dubois et al., 2014). However, to our knowledge, a concise comparative overview

of chemoarchitectonically identified neurons (i.e., neuronal markers) in EC is currently not available.

In the present review, we therefore aim to provide a coherent and up-to-date description of the presence of neuronal markers along with the types of neurons they reveal within EC. Note that this review does not cover markers of inputs to EC and that we do not include activity dependent markers, such as cytochrome oxidase and NADPH diaphorase (information on these aspects in the case of primates and rats can be found in Kobayashi and Amaral, 1999, and Swanson, Köhler, & Björklund, 1987, respectively). Here, we consider different mammalian species from which data are available (Table 1), aiming to highlight both similarities and differences. Further, we discuss how unique populations of principal neurons, and interneurons targeting these, associate with specific neuronal markers and how this may relate to functional characteristics.

2 | DEFINITIONS AND NOMENCLATURE

The literature published on the rodent EC stretches across more than a century and includes a variety of definitions (Canto, Wouterlood, & Witter, 2008). Here, we follow the now generally accepted view of defining EC based on projections to the dentate gyrus that align to a set of cytoarchitectonic features. As detailed descriptions of both rodent and primate EC anchored to this definition are available elsewhere (for rodents, see, for example, Insausti, Herrero, and Witter (1997) and Kjonigsen, Leergaard, Witter, and Bjaalie (2011); for monkeys and humans, see, for example, Amaral, Insausti, and Cowan (1987), Insausti, Munoz-Lopez, Insausti, and Artacho-Perula (2017) and Insausti, Tuñón, Sobreviela, Insausti, and Gonzalo (1995), respectively), we limit the current text to a brief summary. In rodents, EC is situated in a ventroposterior part of the cortical mantle. It borders several cortical areas, such as the piriform cortex anterolaterally, periamygdaloid cortex ventromedially, and the parasubiculum medially. The lateral aspect of EC borders the perirhinal cortex and subsequently the posthinal cortex, when moving along its anterior to posterior extent. In primates, EC is located on the ventromedial surface of the rostral part of the temporal lobe. Here, the rostromedial portion borders the periamygdaloid cortex, and much of its medial part borders the pre- and parasubiculum. The parasubiculum further borders the caudomedial part of EC. Along its rostrolateral and lateral portion, EC borders the perirhinal cortex, whereas the parahippocampal cortex borders the posterior aspects of EC.

Although EC contains six cytoarchitectonically identifiable layers, it is not considered part of the iso- or neocortex as its overall layering appears less developed than that of the neocortex (cf. Stephan, 1975). This review will deal with each layer in detail. To facilitate reading of these detailed laminar descriptions that follow in the main text below, a brief summary of some distinguishing cytoarchitectonic features is presented here. Note that throughout this text, our use of the term *horizontally oriented* refers to elements whose main axis/extent is oriented parallel to the overlying pial surface.

In all mammals, layer I contains a very low number of neurons, but it generally contains dense horizontally oriented neuropil. Layer II contains many large neurons referred to as stellate-neurons ("star-like neurons"), modified pyramidal neurons, and fan neurons, in addition to a relatively sparser presence of smaller bi- and multipolar neurons. In layer III, the most prominent type of neuron has a more archetypical pyramidal morphology that ranges from medium to large in size. Bi-and multipolar neurons are present also in layer III. Unlike the neocortex, EC does not have an internal granule layer. Instead, its layer IV, alternatively called the lamina dissecans ("the cut lamina," as it separates EC into two parts including a superficial part [layers I–III] and a deep part [layers V–VI]), is characterized by dense neuropil and very few neurons. In layer V, the superficial part contains pyramidal neurons of medium to large size that stain darkly with basic dye preparations. Meanwhile, the deep half is characterized by a presence of smaller pyramidal neurons that generally stain lighter. Layer VI contains a mixture of neurons that give this layer a more heterogeneous cytoarchitectonic appearance. The principal types of neurons include pyramidal and multipolar neurons.

For both rodents and primates, alternative division schemes and related nomenclatures for EC have been proposed, see, for example, Insausti et al. (1995), Krimer, Hyde, Herman, and Saunders (1997), Stephan (1975) and von Economo (2009) for humans; Amaral et al. (1987) and Rosene and Van Hoesen (1987) for monkeys; and Blackstad (1956), Insausti et al. (1997) and Wyss (1981) for rats. An extensive description and detailed comparison of all these divisional and nomenclatural schemes is beyond the scope of the present paper. In cases where original studies used different nomenclatures, we have tried to describe the data according to our selected nomenclature, briefly described below. Overall, we aim to describe data in a topographical framework, avoiding complex subdivisional schemes. The use of such a topographical framework, described in more detail in the next section, enables us to compare distributions of identified cell types across species more efficiently.

Traditionally, EC has been considered to comprise two subdivisions, often referred to as Brodman's Area 28 a and b, or lateral and medial entorhinal cortex (LEC and MEC, respectively). The use of area 28 for EC has been largely discontinued, and LEC and MEC has become the more common designation. Data in rodents in particular have provided strong arguments for this bipartition, since

TABLE 1 Main neuroanatomical markers and species covered in this review along with the relevant papers for the entorhinal cortex

Markers	Human	Monkey	Rat	Mouse	Cat	Gerbil	Hedgehog
RE	Herring et al. (2012), Perez-Garcia et al. (2001) and Riedel et al. (2003)	Martínez-Cerdeño et al. (2002)	Drakew et al. (1998), Kitamura et al. (2014), Kobro-Flatmoen et al. (2016), Perez-Garcia et al. (2001), Pesold et al. (1998), Ramos-Moreno et al. (2006) and Varga et al. (2010)	Alcantara et al. (1998), Herring et al. (2012), Kitamura et al. (2014), Kobro-Flatmoen et al. (2016), Leitner et al. (2016) and Miettinen et al. (2005)	Perez-Garcia et al. (2001)	Perez-Garcia et al. (2001)	Perez-Garcia et al. (2001)
CB	Beall and Lewis (1992), Mikkonen et al. (1997, 1999), Naumann et al. (2016), Riedel et al. (2003), Thorns et al. (2001) and Tuñón et al. (1992)	Beall and Lewis (1992), Seress et al. (1994) and Suzuki and Porteros (2002)	Kitamura et al. (2014), Naumann et al. (2016) and Ray et al. (2014)	Fujimaru and Kosaka (1996) and Naumann et al. (2016)			Ferrer et al. (1992)
CR	Brion and Resibois (1994) and Mikkonen et al. (1997, 1999)	Pothuizen et al. (2004) and Seress et al. (1993)	Chaudhuri et al. (2005), Miettinen et al. (1997), Wouterlood et al. (2007), Wouterlood and Härtig (1995) and Wouterlood et al. (2000)				
PV	Arellano et al. (2002), Beall and Lewis (1992), Mikkonen et al. (1997, 1999), Schmidt et al. (1993), Solodkin et al. (1996) and Tuñón et al. (1992)	Beall and Lewis (1992), Berger et al. (1999), Pitkänen and Amaral (1993) and Smaluhn et al. (2000)	Beed et al. (2013), Miettinen et al. (1996), Miettinen et al. (1993), Wouterlood et al. (1995) and Ye et al. (2018)	Fujimaru and Kosaka (1996), Melzer et al. (2012) and Saiz-Sanchez et al. (2012)			
CCK	Lotstra and Vanderhaeghen (1987a,1987b)		Köhler and Chan-Palay (1982)	Phan (2015)			
SOM	Chan-Palay (1987) and Friederich-Ecsy et al. (1988)	Bakst et al. (1985) and Carboni et al. (1990)	Köhler and Chan-Palay (1983), Rogers (1992) and Wouterlood and Pothuizen (2000)				
NPY	Chan-Palay et al. (1986) and Lotstra et al. (1989)	Köhler et al. (1986)	Köhler et al. (1987) and Chan-Palay (1987)				
PSA-NCAM	Murray et al. (2016, 2018) and Varea et al. (2007)		Fox et al. (2000), Foley et al. (2008) and Gomez-Climent et al. (2008)		Varea et al. (2011)		
5HT1aR	Barone et al. (1994)		Chalmers and Watson (1991) and Hammer et al. (1992)				
5HT3aR				Fuchs et al. (2016)			
VGLUT3			Varga et al. (2010)				

(Continues)

WILEY

TABLE 1 (Continued)

Markers	Human	Monkey	Rat	Mouse	Cat	Gerbil	Hedgehog
CB1	Varga et al. (2010)						
VIP			Köhler and Chan-Palay (1983), Loren et al. (1979) and Rogers (1992)	Loren et al. (1979)			
WFA			Lensjø et al. (2017) and Seeger et al. (1994)	Lensjø et al. (2017) and Ueno et al. (2018)			
Wfs1			Kitamura et al. (2014)	Kitamura et al. (2014)			
AChR (multiple)	Graham et al. (2003)		Chaudhuri et al. (2005)				
Enkephalin			Gall et al. (1981)				
SMI-32	Beall and Lewis (1992)	Beall and Lewis (1992) and Lavenex et al. (2009)	Kirkcaldie et al., 2002				
Ctip2			Ohara et al. (2018)				
COX2			Breder et al. (1995)				
Etv1			Ohara et al. (2018)				
nNOS	Egberongbe et al. (1994), Katsuse et al. (2003) and Yew et al. (1999)						

Markers	Odontocete	Ferret	Bat	Wallaby	Pig	Echidna	Guinea pig
RE	Perez-Garcia et al. (2001)	Martinez-Cerdeno et al. (2003)					
CB			Naumann et al. (2016)				
CR					Abraham et al. (2004)		
PV			Gatome et al. (2010)				Uva et al. (2004)
5HT1aR							Sijbesma et al. (1991)
CCK							Köhler and Chan-Palay (1982)
SMI-32			Gatome et al., 2010	Ashwell et al. (2005)		Hassiotis et al. (2004, 2005)	

the two parts can be easily differentiated cytoarchitectonically, and their projections to the dentate gyrus have different zones of termination in the molecular layer (Cappaert et al., 2015; Kjonigsen et al., 2011; Witter, 2007). In primates, several authors have argued that EC clearly shows more than two cytoarchitectonically definable areas, and since the projections to the dentate gyrus predominantly show a more diffuse terminal distribution, this might indicate that further subdivisions are more appropriate. Indeed, seven (monkeys) or eight (humans) subfields have been described within EC on the basis of cytoarchitectonic criteria. Briefly, the olfactory subfield (EO) makes up the rostral-to-rostromedial part of EC, and most of the lateral extent is covered by the lateral rostral (ELR) and the lateral caudal (ELC) subfields. Moving from subfield EO in the caudal direction leads to the rostral subfield (ER) followed by the intermediate subfield (EI); these latter two subfields are situated medially to ELR and ELC, respectively. In monkeys, field EI extends medially until reaching the entorhinal–parasubicular border. However, in humans, a separate entorhinal subfield is recognized medial to EI, referred to as the medial intermediate field (EMI). Finally, the caudal portion of EC includes the caudal (EC) and caudal limiting subfields (ECL). A general awareness of these subfields is of benefit when interpreting results from the literature on EC, and, importantly, it helps to remind us that EC is not a homogeneous structure (Insausti & Amaral, 2012). To parallel this primate scheme in rodents, further subdivisions have been introduced, both for LEC and MEC. Thus, LEC includes a dorsal lateral part (DLE), a dorsal intermediate part (DIE) and a ventral intermediate part (VIE). In turn, MEC includes a medial part (ME) and a caudal part (CE; Insausti et al., 1997). In this review, we do not make use of these schemes but instead, as will be explained in the following section, we place emphasis on domains of EC as they relate to the distance from the collateral sulcus (humans) or rhinal sulcus (monkeys and rodents).

3 | TOPOGRAPHICAL SCHEME RELATED TO THE DISTANCE FROM THE RHINAL/COLLATERAL SULCUS

In rodents, the rhinal sulcus runs along the full dorsolateral limit of EC, thereby constituting a distinct anatomical landmark (Cappaert et al., 2015). A comparable situation is evident in monkeys, where the rhinal sulcus makes up the border of the lateral extent of EC, except at the caudal and dorsal extremes (Amaral et al., 1987). In humans, the collateral sulcus runs along the full lateral and caudolateral extent of EC, approximating the entorhinal–perirhinal border, whereas the rhinal sulcus only borders a small rostrolateral

portion of EC (Figure 1; note that the perirhinal cortex extends slightly medially to the fundus of the collateral sulcus; Insausti & Amaral, 2012). In this review, we place strong emphasis on how, irrespective of subfield, the expression of several neuronal markers changes along a gradient that runs from close to, to increasingly further away from the rhinal sulcus (monkeys and rodents)/collateral sulcus (humans). In our view, this choice not only facilitates species comparisons, but also apparently aligns with the level of cytoarchitectonic differentiation in EC. The latter, likely resulting from developmental processes, results in a gradient such that portions showing the most developed layering are located close to the rhinal/collateral sulcus (Insausti, 1993). In Figure 1, we illustrate this topological framework by indicating the location of the left EC in rats vs humans, along with unfolded map representations of these areas, oriented relative to the rhinal/collateral sulcus and colour-coded to underscore how basic anatomical features are homologous between these species. In this figure, we further attempt to account for recent findings based on fMRI of the human EC, where a separation has been made between the rostrolateral vs caudomedial EC based on preferential connectivity to other brain areas. In particular, the rostrolateral vs caudomedial human EC has a preferential connectivity that is homologous to that of rodent LEC vs MEC, respectively (Maass, Berron, Libby, Ranganath, & Duzel, 2015; Navarro Schroder, Haak, Zaragoza Jimenez, Beckmann, & Doeller, 2015). Interestingly, the areas covered by these entorhinal subfields, that is, LEC and its human homologue and MEC and its human homologue, are comparable between rats and humans, when aligned in relation to the rhinal/collateral sulcus (Figure 1). Furthermore, in Figure 2, we show the distribution of several major neuroanatomical markers as they align to the rhinal/collateral sulcus. In addition, Table 1 provides an overview of the markers covered by this review along with the species from which data on those markers are available.

4 | LAYER I

4.1 | Reelin (RE+)

4.1.1 | Neurons

Layer I contains a sparse population of superficially located RE+ neurons whose morphology appear similar across species (Figure 2a; Martínez-Cerdeño, Galazo, Cavada, & Clascá, 2002; Miettinen et al., 2005; Perez-Garcia et al., 2001; Ramos-Moreno, Galazo, Porrero, Martinez-Cerdeno, & Clasca, 2006; Riedel et al., 2003). In humans, though substantial variation between individuals with respect to the number of RE+ layer I neurons has been reported (Perez-Garcia et al., 2001), vertically oriented mono- and bipolar RE+
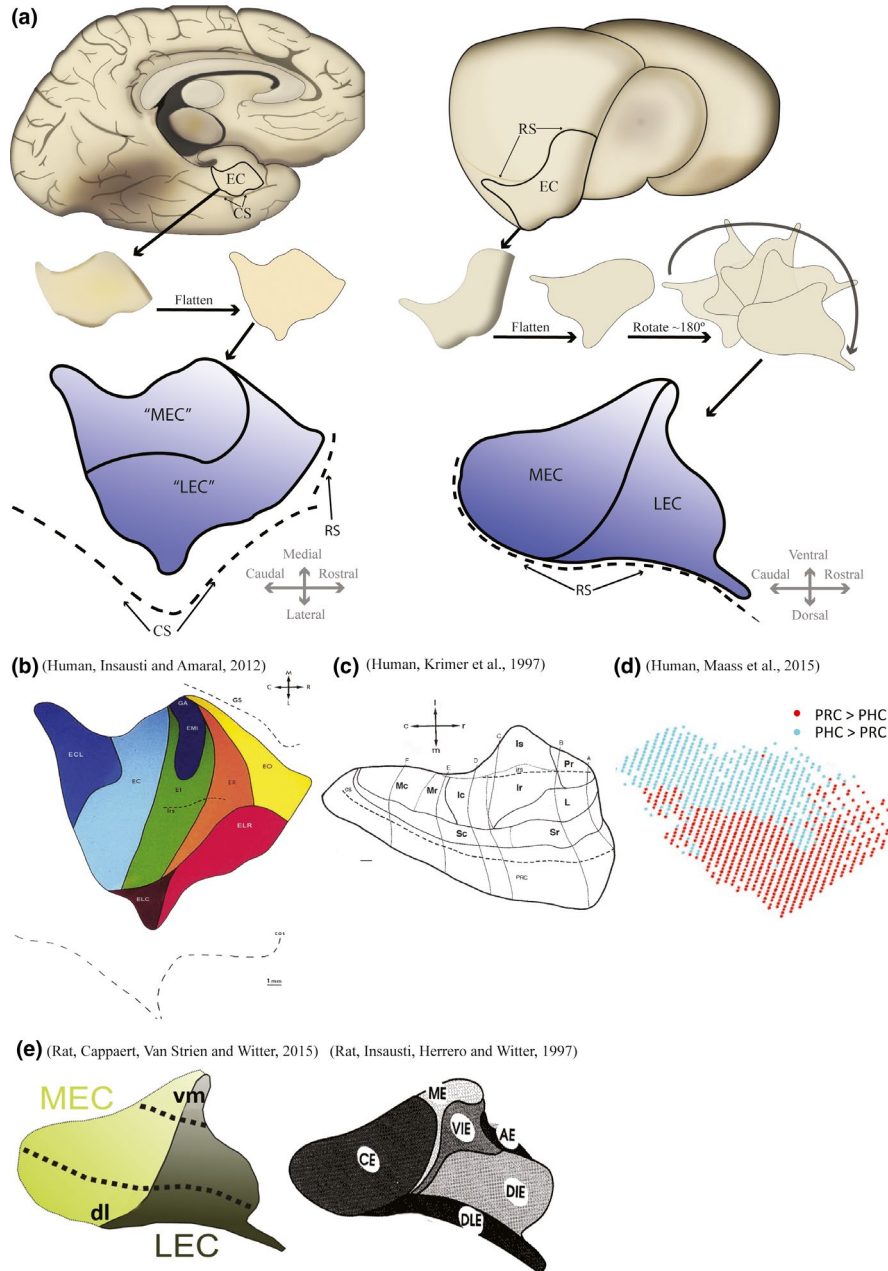
FIGURE 1 Unfolded map representations of the entorhinal cortex (EC). (a) (Top) Illustration of the human (left) and rat (right) brain with the EC delineated, along with indications of the position of the collateral sulcus (CS) and rhinal sulcus (RS). For the human brain, the right hemisphere has been resected to expose the uncus of the medial temporal lobe. (Middle) EC removed from brains and then flattened according to (Cappaert et al., 2015; Insausti & Amaral, 2012; for human vs. rat, respectively). Note that for the rat brain, EC is subsequently rotated about 180° in order to achieve the same orientation as EC in the human brain. (Bottom) higher magnification representation of flattened EC with its two subdivisions lateral entorhinal cortex (LEC) and medial entorhinal cortex (MEC), in relation to the position and extent of CS/RS. The purple shading gradient schematically indicates the postulated gradient in EC of a more developed layering close to the CS/RS (dark) compared to further away from CS/RS (light). This gradient is used to correlate distributional observations of neuroanatomical markers in humans and rodents. (b) The flatmap from (Insausti & Amaral, 2012), whose basic form is used and adapted in this review. (c) An alternative, similar flatmap of EC according to (Krimer et al., 1997). (d) Flatmap rendering of EC from (Maass et al., 2015) indicating the preferred connectivity of caudomedial vs. rostrolateral domains of human EC with parahippocampal vs. perirhinal cortex, respectively. This rendering was superimposed on the flatmap of human EC in (a) in order to derive an approximate border between the human equivalent of MEC vs. LEC (indicated as "MEC and "LEC"). (e) Flatmap of rat EC indicating MEC vs. LEC from (Cappaert et al., 2015) forms the template for rat EC in (a). Also shown is an alternative divisional scheme of rat EC from (Insausti et al., 1997). [Colour figure can be viewed at wileyonlinelibrary.com]

neurons with fusiform somata are generally found (Riedel et al., 2003).

In rats, we find a similarly sparse population of RE+ neurons as well (Figure S1a), apparently with higher numbers in MEC than in LEC (Figure S1b).

4.1.2 | Neuropil

In rats and ferrets, RE+ neuropil are present in layer I of LEC, showing strongest staining in the superficial 1/3, whereas in MEC, such labelling is largely absent except at the portion located furthest away from the rhinal sulcus (Figure 2a; Martinez-Cerdeno, Galazo, & Clasca, 2003; Ramos-Moreno et al., 2006). Neuropil labelling is also present in superficial layer I in monkeys, where potential subfield differences remain to be mapped (Martínez-Cerdeño et al., 2002). In rats, RE+ neuropil appears to coincide with terminations originating in telencephalic olfactory structures, including the olfactory bulb, the anterior olfactory nucleus and the piriform cortex (Cappaert et al., 2015). Since substantial numbers of mitral neurons in the olfactory bulb and pyramidal neurons in the piriform cortex express reelin (Alcantara et al., 1998), it is likely that RE+ fibres in layer I originate, at least in part, from these olfactory domains.

4.2 | Calbindin (CB+)

4.2.1 | Neurons

In humans and monkeys, scattered bipolar and multipolar small or medium sized CB+ neurons reside in layer I (Figure 2b; Mikkonen, Soininen, & Pitkänen, 1997; Suzuki & Porteros, 2002; Riedel et al., 2003). The dendrites of CB+ neurons appear mostly confined within the layer, although dendrites from large neurons occasionally extend into layers II and III, and rarely also into deep layers (Mikkonen et al., 1997; Suzuki & Porteros, 2002; Tuñón, Insausti, Ferrer, Sobreviela, & Soriano, 1992). In contrast, layer I in rodents appears devoid of CB+ neurons (Figure 2b; Fujimaru and Kosaka (1996) and own observations).

4.2.2 | Neuropil

CB+ neuropil in the mouse run deep in layer I in parallel to the pial surface (Fujimaru & Kosaka, 1996). Although a low level of CB+ neuropil is present in humans, monkeys and rats, this organizational feature is not apparent in these latter species (Mikkonen, Alafuzoff, Tapiola, Soininen, & Miettinen, 1999; Mikkonen et al., 1997; Seress, Leranth, & Frotscher, 1994; Suzuki & Porteros, 2002; Tuñón et al., 1992; and own observations)

In both the mouse (Fujimaru & Kosaka, 1996) and the rat, patches of dendritic labelling oriented tangential to the pia are present in layer I, stemming from CB+ pyramidal neurons located in layers II and III (see below). Such patches are most prominent in MEC, but they are also present in domains of LEC located towards the rhinal sulcus (Figures 2b and S2a). Similar dendritic labelling was reported in intermediate and caudal parts of EC in humans and monkeys (Beall & Lewis, 1992; Naumann et al., 2016).

4.3 | Calretinin (CR+)
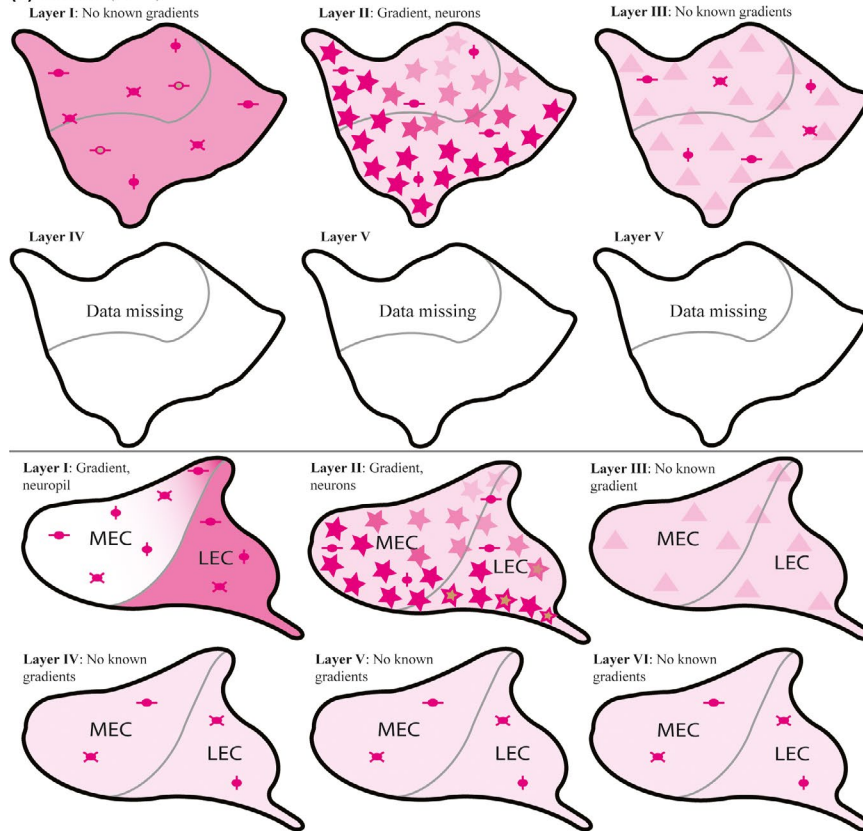
4.3.1 | Neurons

Layer I in humans and monkeys contains a sizable population of medium-to large-sized CR+ bipolar and multipolar neurons, frequently with horizontally oriented thin aspiny dendrites (Mikkonen et al., 1997; Pothuizen, Feldon, & Jongen-Relo, 2004; Seress, Nitsch, & Leranth, 1993). In the rat, morphologically comparable CR+ multipolar neurons, albeit with smaller somata exist. The aspiny dendrites of these neurons extend horizontally for a short distance, eventually turning towards the pia or extending into layer II, occasionally also reaching layer III (Figure 2c; Chaudhuri et al., 2005; Miettinen, Pitkänen, & Miettinen, 1997; Wouterlood, van Denderen, van Haeften, & Witter, 2000).

4.3.2 | Neuropil

A dense band of horizontally oriented CR+ neuropil is present superficially in layer I in both humans (Mikkonen et al., 1997) and monkeys (Pothuizen et al., 2004). The more detailed descriptions available for humans show that such CR+ neuropil are particularly dense in domains located furthest away from the collateral sulcus, with gradually decreasing density when moving successively closer to the collateral sulcus (Figure 2c; Mikkonen et al., 1997). In the rat, CR+ neuropil are present in the superficial half of layer I in LEC, and labelling decreases when entering MEC such that only

FIGURE 2 Summary panels for neuroanatomical markers in the entorhinal cortex (EC) of primates and rodents. The distribution of the neuroanatomical markers reelin (a), calbindin (b), calretinin (c), parvalbumin (d), cholecystokinin (e), somatostatin (f) and neuropeptide Y (g) are indicated on schematics of the human (top rows) vs. rodent EC (bottom rows; see Figure 1 for indication of how the schematics map onto the human vs. rodent brain). Details about the neuronal morphologies are indicated where this is known (right columns). Differing colour intensities for both neurons and neuropil indicate expression levels of the respective markers. Key references for each marker are listed in the bottom right of each panel. [Colour figure can be viewed at wileyonlinelibrary.com]

(a) Reelin (RE+)

Layer I: No known gradients   **Layer II**: Gradient, neurons   **Layer III**: No known gradients

Layer IV   **Layer V**   **Layer V**

Data missing   Data missing   Data missing

Layer I: Gradient, neuropil   **Layer II**: Gradient, neurons   **Layer III**: No known gradient

MEC / LEC   MEC / LEC   MEC / LEC

Layer IV: No known gradients   **Layer V**: No known gradients   **Layer VI**: No known gradients

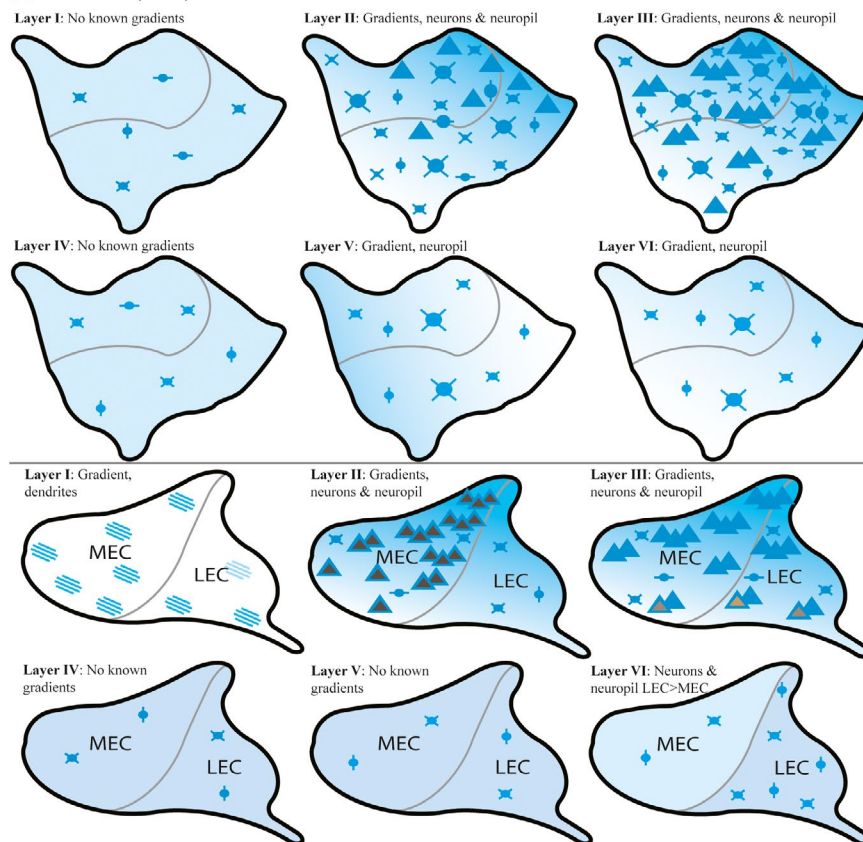MEC / LEC   MEC / LEC   MEC / LEC

Legend (RE+):

- ● / ◆ Small-medium mono/bipolar
  Soma: 5–15 μm in both axes
  Dendritic extent: confined to parent layer
  Spines: No
  - ⊶ Co-express calretinin
    (5–15 μm in both axes)
- ✳ Small multipolar
  Soma: 5–15 μm in both axes
  Primary dendrites: data missing
  Dendritic extent: data missing
  Spines: no
- ★ Large stellate or fan
  Soma: 20–25 μm x 10–18 μm
  Primary dendrites: 4–11
  Dendritic orientation: mixed
  Dendritic extent: cross adjoining layers; note that superficially oriented dendrites are extensive
  Spines: yes
  - ☆ Co-express enkephalin (fan)
- ▲ Pyramidal (weak labeling)
  See description for CB+ pyramidal neurons

References for RE+ neurons

Klink and Alonso (1997); Pesold et al. (1998); Alcantara et al. (1998); Drakew et al. (1998); Perez-Garcia et al. (2001); Martinez-Cerdeno et al. (2003); Miettinen et al. (2005); Ramos-Moreno et al. (2006); Stranahan et al. (2010); Canto and Witter (2012a); Canto and Witter (2012b); Varga et al. (2010); Kitamura et al. (2014)
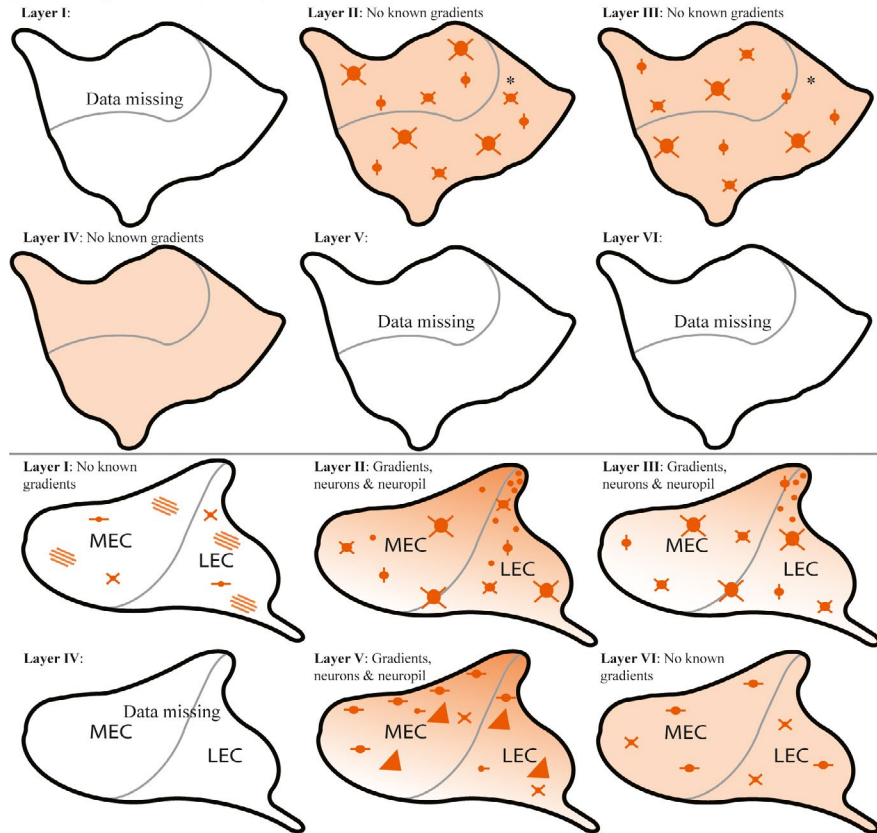
(b) Calbindin (CB+)

Layer I: No known gradients   **Layer II**: Gradients, neurons & neuropil   **Layer III**: Gradients, neurons & neuropil

Layer IV: No known gradients   **Layer V**: Gradient, neuropil   **Layer VI**: Gradient, neuropil

Layer I: Gradient, dendrites   **Layer II**: Gradients, neurons & neuropil   **Layer III**: Gradients, neurons & neuropil

MEC / LEC   MEC / LEC   MEC / LEC

Layer IV: No known gradients   **Layer V**: No known gradients   **Layer VI**: Neurons & neuropil LEC>MEC

MEC / LEC   MEC / LEC   MEC / LEC

Legend (CB+):

- ● / ◆ Small-medium bipolar, horizontal/vertical
  Soma: 10–14 μm in either axis
  Dendritic extent: confined to parent layer
  Spines: no
- ● / ◆ Large bipolar
  Soma: Up to 30 μm in long axis
  Dendritic extent: reach adjoining layers
  Spines: no
- ✕ Small multipolar
  Soma: up to 10 μm in both axes
  Primary dendrites: 3–5
  Dendritic extent: confined to parent layer
  Dendritic orientation: mixed
  Spines: no
- ✳ Medium multipolar
  Soma: 11–19 μm x 8–16 μm
  Primary dendrites: 3–5
  Dendritic extent: mainly confined to parent layer
  Dendritic orientation: mixed
  Spines: few or none
- ✖ Large multipolar
  Soma: 20–30 μm x 11–20 μm
  Primary dendrites: 3–5
  Dendritic extent: reaches adjoining layers
  Dendritic orientation: mixed
  Spines: few or none
- ▲ Pyramidal
  Soma: 20–25 μm x 12–16 μm
  Primary dendrites: 1 apical, 3–5 basal
  Dendritic extent: apical dendrite reaches layer(s) above, basal dendrites often remain in parent layer
  Spines: yes
  - ▲ Co-express COX2; ▲ Wolfram syndrome 1-protein; ▲ enkephalin
- 〰 Cb-IR ascending dendrites (from layer II)

References for CB+ neurons

Beall and Lewis (1992); Tunon et al. (1992); Seress et al. (1994); Fujimaru and Kosaka (1996); Mikkonen et al. (1997); Mikkonen et al. (1999); Suzuki and Porteros (2002); Kjonigsen et al. (2011); Kitamura et al. (2014); Gianatti (2015)
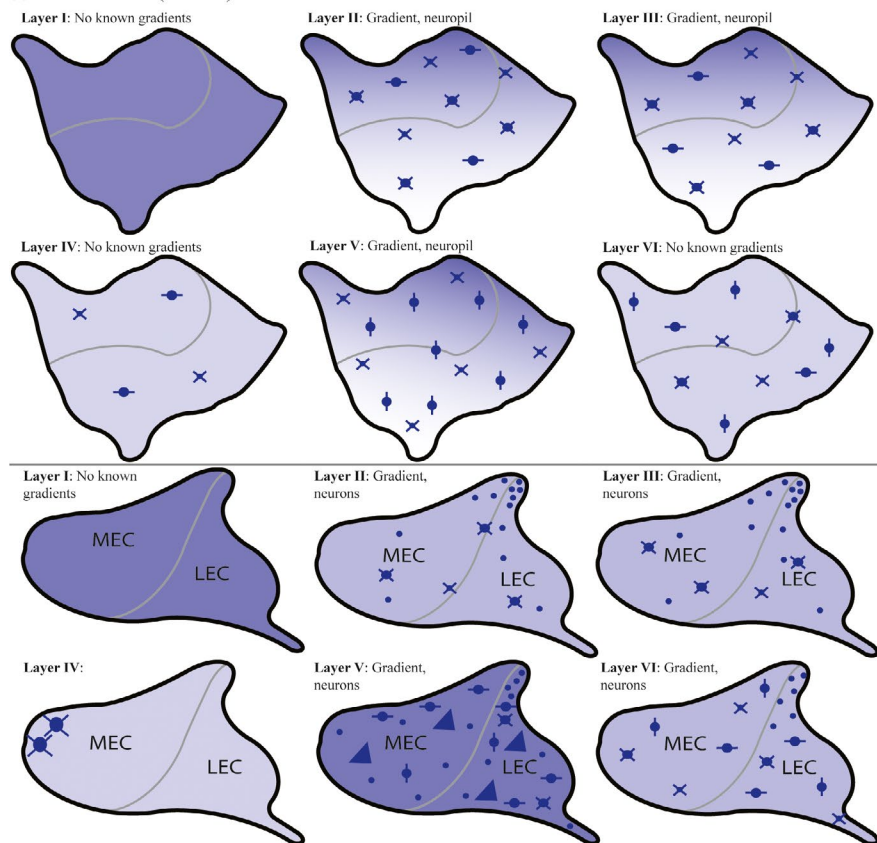
FIGURE 2 (Continued)

(e) Cholecystokinin (CCK+)

Layer I: Data missing
Layer II: No known gradients
Layer III: No known gradients
Layer IV: No known gradients
Layer V: Data missing
Layer VI: Data missing

Layer I: No known gradients — MEC / LEC
Layer II: Gradients, neurons & neuropil — MEC / LEC
Layer III: Gradients, neurons & neuropil — MEC / LEC
Layer IV: Data missing — MEC / LEC
Layer V: Gradients, neurons & neuropil — MEC / LEC
Layer VI: No known gradients — MEC / LEC

- Small round/oval with undefined processes
  Soma: up to 10 μm in both axes
- Small unipolar
  Soma: up to 10 μm in both axes)
- Small bipolar
  Soma: approximately 10 μm in both axes
  Dendritic extent: known to extend for long distances*
- Medium bipolar
  Soma: approximately 20 μm in both axes
  Dendritic extent: (LIII) vertically oriented ones reach layer I and likely also layer V
- Small multipolar
  Soma: approximately 10 μm in both axes
  Primary dendrites: 3–?
  Dendritic extent: data missing
  Spines: data missing
- Medium multipolar
  Soma: approximately 20 μm in both axes
  Primary dendrites: 3–?
  Dendritic extent: data missing
  Dendritic orientation: data missing
  Spines: data missing
- Large multipolar
  Soma: up to 30 μm in either axis
  Primary dendrites: 3–?
  Dendritic extent: reaches adjoining layers; certain dendrites observed to extend across all layers may emanate from this neuron type*
  Dendritic orientation: mixed
  Spines: data missing
- Pyramidal/pyramidal-like
- CCK: ascending dendrites

Note: The majority of CCK-IR neurons also express CB1 and 5HT3A, plus VGLUT3 on their axon terminals

References for CCK+

Kohler and Chan-Palay (1982)*; Lotstra and Vanderhaeghen (1987a); Lotstra and Vanderhaeghen (1987b)

(f) Somatostatin (SOM+)

Layer I: No known gradients
Layer II: Gradient, neuropil
Layer III: Gradient, neuropil
Layer IV: No known gradients
Layer V: Gradient, neuropil
Layer VI: No known gradients

Layer I: No known gradients — MEC / LEC
Layer II: Gradient, neurons — MEC / LEC
Layer III: Gradient, neurons — MEC / LEC
Layer IV: — MEC / LEC
Layer V: Gradient, neurons — MEC / LEC
Layer VI: Gradient, neurons — MEC / LEC

- Small round/oval with undefined processes
  Soma: approximately 10 μm in both axes
- Small-medium bipolar
  Soma: 10–20 μm in long axis
  Dendritic extent: data missing
  Spines: no
- Small multipolar
  Soma: less than 15 μm in either axis
  Primary dendrites: 3–4
  Dendritic extent: data missing
  Dendritic orientation: mixed
  Spines: no
- Medium multipolar
  Soma: 15–25 μm in long axis
  Primary dendrites: 3–4
  Dendritic extent: data missing
  Dendritic orientation: mixed
  Spines: no
- Large multipolar
  Soma: up to 30 μm in long axis
  Primary dendrites: 3–4
  Dendritic extent: cross adjacent layers
  Dendritic orientation: mixed
  Spines: no
- Pyramidal/pyramidal-like
  Soma: located in superficial parts of layer V*, morphological details missing

References for SOM+

Kohler and Chan-Palay (1983)*; Bakst et al. (1985); Chan-Palay (1987)**; Friederich-Ecsy et al. (1988); Carboni et al. (1990); Wouterlood and Pothuizen (2000)

FIGURE 2 (Continued)

(g) Neuropeptide Y (NPY+)
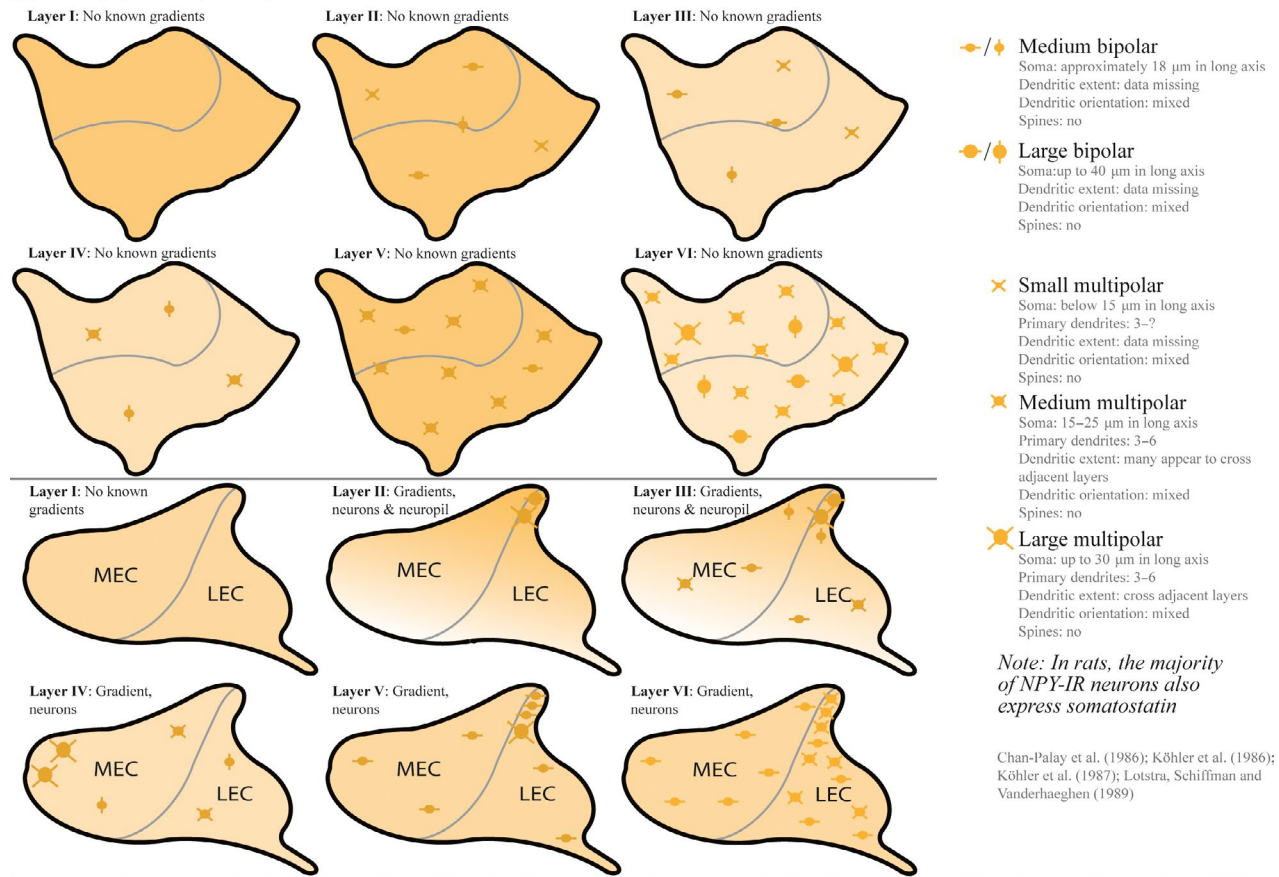
FIGURE 2 (Continued)

sparse labelling is present in the domains located close to the rhinal sulcus (Miettinen et al., 1997; Wouterlood et al., 2000). In this species, part of the CR+ neuropil is known to comprise fibres originating from the olfactory bulb (Wouterlood & Härtig, 1995).

4.4 | Parvalbumin (PV+)

4.4.1 | Neurons

Studies in mice, rats, bats, guinea pigs, monkey and humans report that layer I is devoid of PV+ somata (Beall & Lewis, 1992; Berger, De Grissac, & Alvarez, 1999; Gatome, Slomianka, Mwangi, Lipp, & Amrein, 2010; Miettinen, Koivisto, Riekkinen, & Miettinen, 1996; Miettinen et al., 1993; Mikkonen et al., 1997, 1999; Saiz-Sanchez, Ubeda-Banon, De la Rosa-Prieto, & Martinez-Marcos, 2012; Smaluhn, Plaschke, Leranth, & Nitsch, 2000; Solodkin, Veldhuizen, & Van Hoesen, 1996; Tuñón et al., 1992; Uva, Gruschke, Biella, De Curtis, & Witter, 2004; Wouterlood, Härtig, Brückner, & Witter, 1995). However, in some studies in humans and monkeys, a class of small, bipolar or multipolar PV+ neurons were reported (Pitkänen & Amaral, 1993; Schmidt, Braak, & Braak, 1993). The discrepancy between

studies might represent a potential preferred position of these neurons across the surface of EC since in the monkey (Pitkänen & Amaral, 1993), these small multipolar neurons are rare in rostral portions, with an increasing presence at more caudal levels (Figure 2d).

4.4.2 | Neuropil

PV+ neuropil labelling in EC-layer I of humans is moderate at rostrolateral, caudolateral and intermediate subfields (Mikkonen et al., 1997; Tuñón et al., 1992). Different studies have reported different results with respect to the intralayer location of such fibres, ranging from superficial (Tuñón et al., 1992), to middle (Schmidt et al., 1993), to deep (Mikkonen et al., 1997). This likely reflects differences between different EC subfields. In both monkeys (Pitkänen & Amaral, 1993) and rodents (Fujimaru & Kosaka, 1996; Miettinen et al., 1996; Wouterlood et al., 1995), neuropil labelling in layer I appears weak (Figure 2d).

4.5 | Cholecystokinin (CCK+)

In rats and guinea pigs, a low number of small multipolar and horizontally oriented bipolar CCK+ somata and dendrites are

present in layer I (Köhler & Chan-Palay, 1982; Phan, 2015). In mice, a cluster of CCK+ neurons appears to reside in the portion of LEC located close to the rhinal sulcus, abutting the border with the perirhinal cortex (Phan, 2015). Whether this feature is present in other species remains to be explored. CCK+ neuropil have been identified as dendrites originating from neurons in deep layers (Figure 2e; Köhler & Chan-Palay, 1982).

4.6 | Somatostatin (SOM+) and Neuropeptide Y (NPY+)

Irrespective of species, layer I is essentially devoid of SOM+ as well as NPY+ neurons. However, antibodies against both molecules each densely label neuropil within this layer (Figure 2f,g), which appears to originate from neurons situated in deeper layers (Bakst, Morrison, & Amaral, 1985; Carboni, Lavelle, Barnes, & Cipolloni, 1990; Chan-Palay, 1987; Friederich-Ecsy, Braak, Braak, & Probst, 1988; Köhler & Chan-Palay, 1983; Wouterlood & Pothuizen, 2000). In the case of SOM+ neuropil in layer I, many are axons arising from Martinotti cells situated in deeper layers, in particular layer III (Tahvildari, Wolfel, Duque, & McCormick, 2012), but possibly also layer V as is seen in the neocortex (Silberberg & Markram, 2007; Wang et al., 2004).

4.7 | Co-localization

The horizontally oriented bipolar type of RE+ layer I neurons co-localize with CR+, at least in humans (Figure 2a; Riedel et al., 2003). In both rats (Miettinen et al., 1997) and monkeys (Pothuizen et al., 2004), virtually all CR+ layer I-neurons reportedly stain positive for γ-aminobutyric acid (GABA+) or glutamic acid decarboxylase (GAD+). However, another report in the rat found less than one-third of the CR+ layer I-neurons to be GABA+ (Wouterlood et al., 2000). This discrepancy is likely the result of methodological differences. Layer I in rats also contains VIP+ neurons (Köhler & Chan-Palay, 1983). Appearing small and with horizontally oriented thin aspiny dendrites, these neurons bear a striking resemblance to the CR+ neurons found in this layer (compare figure 5g in Köhler & Chan-Palay, 1983, with figure 5a in Miettinen et al., 1997, figure 4b in Wouterlood et al., 2000, and figure 9a in Mikkonen et al., 1997). This is in line with the more general observation that the majority of CR+ neurons in EC stain positive for VIP (Rogers, 1992). Also, muscarinic acetylcholine receptor type 2 (m2AChR) is expressed by at least two-thirds of the CR+ layer I-neurons (Chaudhuri et al., 2005).

Work on mice shows that the superficial portion of layer I labels positive for *Wisteria floribunda* agglutinin (WFA), indicating the presence of perineuronal nets. However, immunolabelling against aggrecan, considered the main chondroitin sulphate proteoglycan of most if not all perineuronal nets, appears to be present at only low amounts (Ueno et al.,

2018). This is in line with previous reports on perineuronal nets in rodent EC showing that they are present at low levels in EC compared with most other cortical areas (Seeger, Brauer, Härtig, & Brückner, 1994).

4.8 | Conclusions, layer I

Data on the chemical nature of neurons in layer I across species are sparse, but it is apparent that overall similarities are strong.

5 | LAYER II

Currently, two schemes for delineating EC-layer II/III in rodents are in frequent use. The first of these two schemes follow the original definition by Cajal and Lorente de Nó, who emphasized that layer II is rather narrow and dominated by neurons with a stellate morphology. These authors further noted that layer II also contains pyramidal-like neurons with apical dendrites oriented obliquely towards the pia, plus occasional classical pyramidal neurons, with both groups being interspersed among the stellate neurons. Layer III, as originally defined by these authors, is broad and dominated by several strata of pyramidal neurons, with relatively small to medium sized pyramidal neurons located towards the border with layer II, although slightly larger pyramidal neurons are present towards the border with layer IV (Figure 3a; Cajal, 1901; Lorente de Nó, 1933).

The second scheme for delineating EC-layer II/III that is currently in use, suggests that layer II is much wider than that of the original definition. According to the alternative scheme, layer II includes the small to medium sized pyramidal neurons originally defined as belonging to superficial layer III. This alternative scheme further posits that in the dorsal part of LEC, layer II splits into two sublayers. Here, the outer sublayer, including the fan cells characteristic of LEC, is referred to as layer IIa, and the inner sublayer, consisting of pyramidal cells, is referred to as layer IIb (Figure 3b).

In this review, we adhere to the original definition of EC-layer II/III by Cajal and Lorente de Nó, but for the sake of clarity, we will point out instances when superficial layer III-neurons are located at positions alternatively referred to as layer IIb.

5.1 | Reelin (RE+)

5.1.1 | Neurons

Work in several species, including the mouse, rat, gerbil, hedgehog, ferret, cat, dolphin, whale and humans, has established that layer II of EC contains a large population of RE+ neurons. Of these, a few are small multipolar
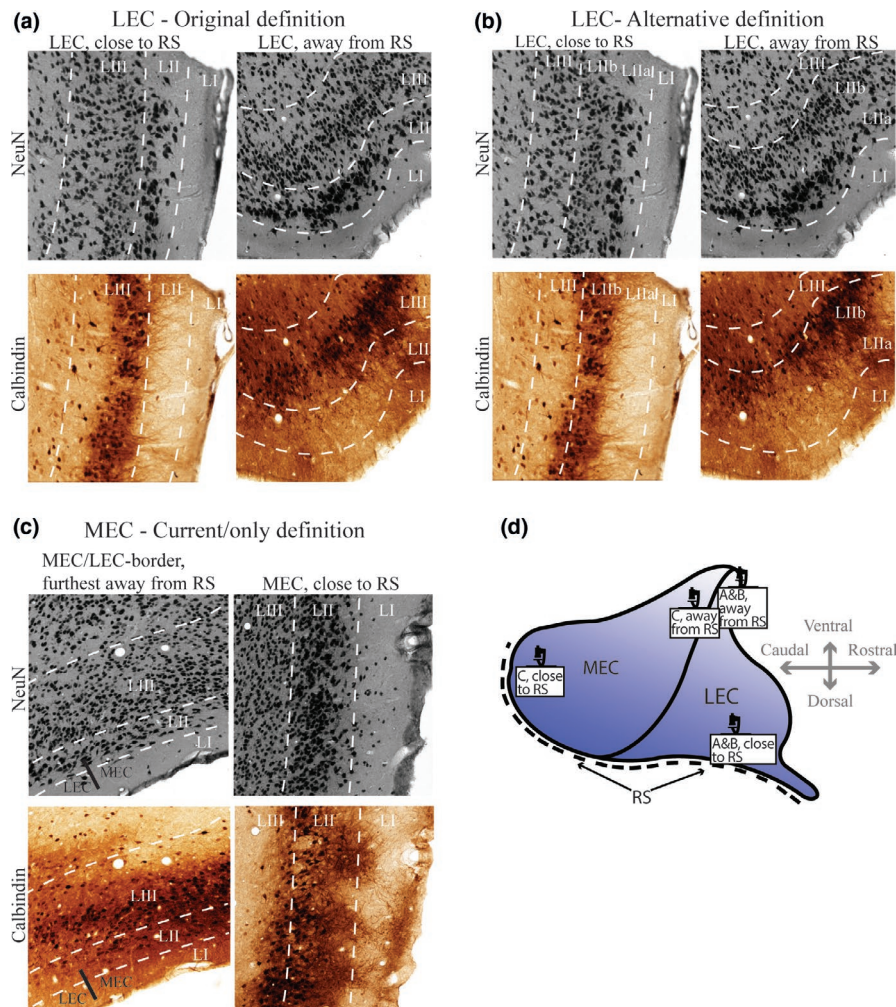
FIGURE 3 Designating calbindin-positive (CB+) pyramidal neurons in rat lateral entorhinal cortex (LEC) as layer II vs. layer III-neurons depends on whether the original or an alternative laminar scheme is used. (a) As originally defined by Cajal and Lorente dé No, layer II of the entorhinal cortex (EC) is more narrow than layer III. Moreover, layer II is dominated by stellate cells and layer III is dominated by relatively small pyramidal cells. This definition delineates LEC-layer II as exemplified in the domain close to the rhinal sulcus (RS) vs. away from RS after NeuN staining (top panels). Adjacent CB+ immunoperoxidase-labelled sections show that layer II of LEC is essentially devoid of CB+ neurons when following the original definition (bottom panels). (b) An alternative scheme of delineation suggests that layer II of LEC is wider than in the original definition and that it consists of two sublayers, IIa and IIb (top panels). This implies that layer II of LEC contains a large population of CB+ neurons (bottom panels). (c) In medial entorhinal cortex (MEC), many CB+ neurons situate in layer II whether one follows the current (and only) definition or places the layer II/III border at a deeper position. NeuN-labelled examples of the domain of MEC located furthest away from RS and thus bordering LEC vs. domains of MEC located closer to RS (top panels) are contrasted with adjacent immunoperoxidase-labelled CB+ neurons (bottom panels). Note the gradual appearance of superficial CB+ neurons when moving from the domain located furthest away from RS in LEC vs. the domain located furthest away from RS in MEC (i.e., the border region). For each panel, the layers are indicated with dashed lines. Panels are based on sections adapted from the Rat Hippocampus Atlas (Kjonigsen et al., 2011), taken from the following Bregma levels: (a,b) close to RS 6.76, away from RS 7.48; (c) MEC/LEC border 7.66, MEC close to RS 8.02. (d) Flatmap of rat EC showing the location represented by each image in (a–c). [Colour figure can be viewed at wileyonlinelibrary.com]

or fusiform neurons likely constituting interneurons (Martinez-Cerdeno et al., 2003; Perez-Garcia et al., 2001; Ramos-Moreno et al., 2006). The majority of layer II RE+ neurons coincide with the morphologically described stellate and fan cells (Alcantara et al., 1998; Drakew, Frotscher, Deller, Ogawa, & Heimrich, 1998; Kitamura et al., 2014; Martinez-Cerdeno et al., 2003; Perez-Garcia et al., 2001; Pesold et al., 1998; Varga et al., 2010), although a better description likely is that reelin is selectively expressed

in neurons that give rise to projections to DG and CA3 (Kitamura et al., 2014; Leitner et al., 2016; Varga et al., 2010; Witter, Doan, Jacobsen, Nilssen, & Ohara, 2017). The same is likely the case for layer II neurons targeting CA2. This is in line with work showing that reconstructed single stellate neurons in MEC project to DG, and also to CA3 and CA2 (Tamamaki & Nojyo, 1993), and is reinforced by the non-GABAergic chemoarchitecture of the RE+ somata (Alcantara et al., 1998) and the RE+

terminal distributions in the hippocampus (Herring et al., 2012; Miettinen et al., 2005; Ramos-Moreno et al., 2006). Neurons located close to the rhinal sulcus (monkeys and rodents) or collateral sulcus (humans) express higher levels of reelin than those located successively further away from the rhinal/collateral sulcus (Figure 2a; Perez-Garcia et al., 2001; Kobro-Flatmoen, Nagelhus, & Witter, 2016).

5.1.2 | Neuropil

RE+ neuropil is present at moderate density in EC-layer II. Notably, the axons of RE+ layer II-neurons are immunoreactive for reelin (Martinez-Cerdeno et al., 2003, own unpublished observations).

5.2 | Calbindin (CB+)

5.2.1 | Neurons

A description of the distribution of CB+ pyramidal neurons in layer II in rodents requires particular precision due to the present use of two different schemes for delineating layer II from layer III. This issue mainly concerns LEC, where adherence to one over the other scheme positions CB+ pyramidal neurons to either layer IIb or superficial layer III. The original definition by Cajal and Lorente de Nó implies that unlike for MEC, layer II of LEC is devoid of CB+ pyramidal neurons (Figures 2b and 3a,c). The alternative delineation places a sizable population of superficial LEC CB+ pyramidal neurons in layer II, in what is then referred to as layer IIb (Figure 3b). Note that in the case of mouse LEC, CB+ pyramidal neurons in ventral and intermediate parts situate more superficially and fall within layer II for either scheme of delineation (Figure 4a). In contrast, in dorsolateral LEC in mice, CB+ pyramidal neurons are located at a depth comparable to that in LEC of rats, that is, deep to the RE+ neurons (Figure 4b).

In MEC of both rats and mice, CB+ pyramidal neurons are present in layer II irrespective of whether one adheres to the original definition or choses to place the border with layer III at a deeper position, although for MEC in rats, placing the border at a deeper position will include more such neurons to layer II (Figure 3c). Also note that in MEC of mice, CB+ neurons are located superficial to RE+ neurons; thus, the relative position of these neuronal types is inverted in mice compared to rats (Figure 4c). Moreover, in mice, the majority of CB+ neurons in layer II of MEC reside in clusters, thus giving a patch-like appearance (Fujimaru & Kosaka, 1996), and a similar feature is present in rats (Figures 3c and S2a). Likely, the majority of neurons in these clusters constitute pyramidal neurons, and many have strongly CB+ apical dendrites reaching into layer I (Kitamura et al., 2014; Ray et al., 2014). Similar findings have been reported for humans (Mikkonen et al., 1997; Naumann et al., 2016; Thorns,

Licastro, & Masliah, 2001) and monkeys (Beall & Lewis, 1992), where such patches have been observed throughout EC. Reports on humans and monkeys indicate a numerical decrease of CB+ pyramidal neurons in layer II from areas close to the rhinal/collateral sulcus towards more distal locations, without a clear parallel change in the total number of CB+ neurons (Figure 2b; Mikkonen et al., 1997; Suzuki & Porteros, 2002). Thus, a higher proportion of non-pyramidal CB+ neurons reside in these more distal locations, likely represented by multipolar and bipolar neurons. As summarized in Figure 2b, the overall size, shape and distribution of the latter types are highly similar across species, although note that in humans, large multipolar neurons reside mainly in the deep part of the layer (Beall & Lewis, 1992; Tuñón et al., 1992), whereas in monkeys, such neurons appear homogenously distributed throughout the depth of the layer (Suzuki & Porteros, 2002). Meanwhile, medium-sized multipolar CB+ neurons mainly reside within the classic stellate cell islands, at least in humans (Beall & Lewis, 1992; Mikkonen et al., 1997; Seress et al., 1994; Suzuki & Porteros, 2002; Tuñón et al., 1992).

In EC of rodents, CB+ multipolar neurons were recently described in superficial layer III (layer IIb) of LEC (Leitner et al., 2016), but CB+ bipolar neurons have not previously been described. Using the Rat Hippocampus Atlas available through the Rodent Brain Workbench (RBWB.org; see Kjonigsen et al., 2011), we confirmed the presence of CB+ multipolar neurons in layer II (Figure S2c) and observed CB+ bipolar neurons in this layer (Figure S2d) as well as in layers III-VI (see below). CB+ multipolar neurons appear to make up a very sparse population, and only the proximal part of their dendrites contains labelling (Figure S2c). CB+ multipolar neurons have also been reported in EC of the hedgehog (Ferrer, Zujar, Admella, & Alcantara, 1992). The density of CB+ bipolar neurons in EC layer II (and III) in the rat appears lower than in humans and non-human primates (see above paragraph), as well as compared with superficial layers of the neocortex in rats (Figure 2b; Celio, 1990).

5.2.2 | Neuropil

CB+ neuropil in EC-layer II of humans and monkeys are slightly more prominent rostrally than caudally (Mikkonen et al., 1997; Suzuki & Porteros, 2002). In rats and mice, such labelling appears most pronounced ventrally, that is, away from the rhinal sulcus (Figure 2b; Fujimaru & Kosaka, 1996, and own unpublished observations).

5.3 | Calretinin (CR+)

5.3.1 | Neurons

In EC-layer II of humans (Mikkonen et al., 1997), monkeys (Pothuizen et al., 2004; Seress et al., 1993), rats (Miettinen
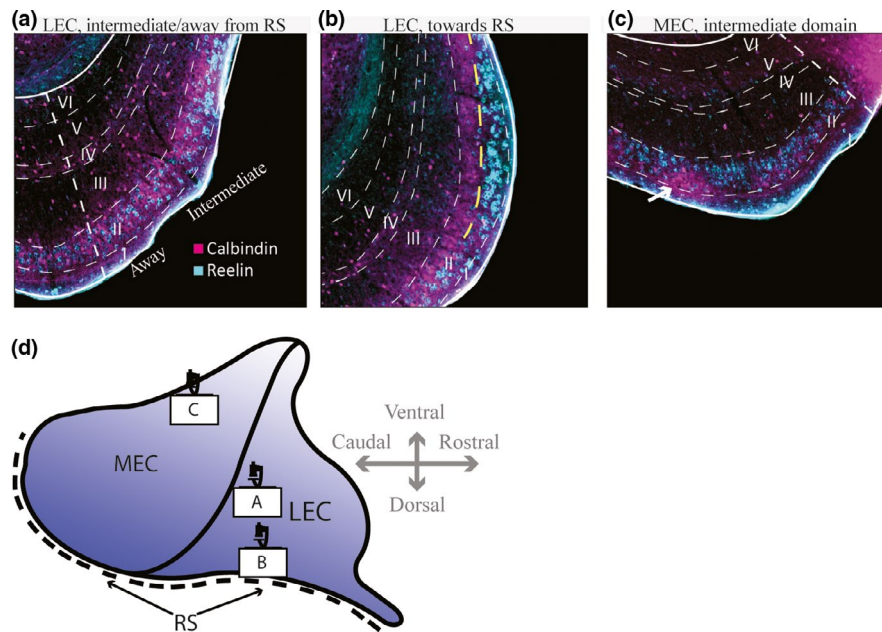
FIGURE 4 Distribution of calbindin-positive pyramidal neurons, compared to that of reelin positive neurons in entorhinal cortex (EC)-layer II and III of the mouse. (a) In domains intermediate and furthest away from the rhinal sulcus (RS) of the lateral entorhinal cortex (LEC), CB+ pyramidal neurons (magenta) are located in layer II at a similar depth as reelin positive (RE+) neurons (cyan). (b) Moving increasingly towards RS in LEC, CB+ pyramidal neurons are situated increasingly deeper, such that according to the original definition by Cajal and Lorente de Nó, such neurons in the domain bordering RS likely belong to layer III. Note that the border between layers II and III according to the original definition is shown as a yellow dashed line, and the alternative definition is indicated by the white dashed lines. (c) In mouse medial entorhinal cortex (MEC), layer III is virtually devoid of CB+ pyramidal neurons. Conversely, superficial layer II contains multiple clusters of such neurons (arrow). Cell types are coloured the same way for all figures and labelling is based on immunofluorescence. Adapted from Witter et al. (2017) with permission from the author. (d) Flatmap of rat EC (from Figure 1 which is based on the rat, but is essentially the same for mice) showing the location represented by each image in (a–c). [Colour figure can be viewed at wileyonlinelibrary.com]

et al., 1997; Wouterlood et al., 2000, 2007) and pigs (Abraham, Toth, & Seress, 2004), a sizable population of CR+ neurons is present, including small- and medium-sized multipolar neurons and small bipolar neurons. In rats, large CR+ multipolar neurons have also been described (Figure 2c).

5.3.2 | Neuropil

In human EC, labelling in layer II is dense in the domains that are located furthest away from the collateral sulcus and tapers off when moving successively closer to the collateral sulcus (Mikkonen et al., 1997). In the rat, layer II appears nearly devoid of CR+ neuropil (Figure 2c; Miettinen et al., 1997; Wouterlood et al., 2000).

5.4 | Parvalbumin (PV+)

A strong gradient of immunoreactivity to PV+ is present between and even across subfields in all species studied. Labelling intensity is much higher closer to the rhinal/collateral sulcus than in parts of EC further away from the sulcus. Labelling density is comprised of two elements, somata and neuropil. With respect to somata, this gradient is well established in humans and non-human primates, such that

very few PV+ neurons are detectable in the domains located furthest away from the rhinal/collateral sulcus, in contrast to areas located increasingly closer to the sulcus (Figure 2d; Beall & Lewis, 1992; Mikkonen et al., 1997, 1999; Pitkänen & Amaral, 1993; Schmidt et al., 1993; Tuñón et al., 1992).

In the case of rodents, such a gradient in cell numbers is more debated, particularly in the case of MEC-layer II (as well as in layer III). A recent paper reported that in MEC of rats, the density of PV+ somata is nearly constant irrespective of the position along this axis, though the PV+ axon density is higher in the dorsal portion (close to the sulcus) than in the ventral portion (Beed et al., 2013). This contrasts with a previous study in mice (Fujimaru & Kosaka, 1996) that reported a gradient for PV+ somata similar to that reported in other species, that is, outside of the rat. However, our own observations in rats are in line with reports in humans, monkeys and mice. We used rat tissue containing MEC-layer II immunolabelled against PV+, including coronal (16 sections from two animals) and sagittal sections (seven sections from one animal). On each section, we delineated the full extent of MEC-layer II by overlaying adjacent NeuN-stained sections. Subsequently, we divided layer II into three equally sized portions, that is, the dorsal 1/3, the intermediate 1/3 and the ventral 1/3.

Using ImageJ (NIH, Version 1.43 m), photomicrographs of every section were converted to 8-bit greyscale images before a threshold was set to filter out neuropil, leaving only the contours of somata (i.e., cell profiles). After calibrating the particle analyser tool in ImageJ to recognize PV+ somata, based on visual inspection of control sections before and after thresholding, we used this tool on every portion from every section to count somata (dorsal 1/3, N = 808, mean 35,1, standard deviation (SD) 15,1; intermediate 1/3, N = 554, mean 24,1, SD 15,1; ventral 1/3, N = 308, mean 13,4, SD 12,3). The counts were found to be normally distributed and of homogenous variance. A two-way analysis of variance showed that there was no significant difference in the number of neurons between the animals ($p = .12$) or animal × level (0.68). The same analysis showed that there was a significant difference in the number of neurons depending on the distance from the rhinal sulcus. Specifically, a post hoc multiple comparisons test (Tukey's test) revealed a significant drop in the number of PV+ cell profiles in the most distant 1/3 compared with the intermediate 1/3 (44%, $p = .036$) and the closest 1/3 (62%, $p < .001$), and the intermediate 1/3 also had significantly fewer such neurons than the closest 1/3 (31%, $p = .029$; Figure 5a–c). A similar gradient has also been observed in LEC of rats (Wouterlood et al., 1995), and our own observations are in agreement with this (Figure 5d). Based on this, we conclude that the density of PV+ somata in both MEC and LEC of the rat follows the same topological gradient as that reported for humans, monkeys and mice (Figure 2d).

5.4.1 | Neurons

Morphological data on PV+ neurons are available from humans, monkeys, rats, mice and bats. Such neurons in EC-layer II are bipolar and multipolar, range from very small to large and have dendrites with moderate arborization. Overall, the PV+ neuron types and their distribution are highly similar across species (Figure 2d), although a few differences are notable. For example, in the case of humans and monkeys, dendrites from large PV+ multipolar neurons moderately arborize into secondary dendrites of which some ascend to layer I and others descend into layer III (Beall & Lewis, 1992; Fujimaru & Kosaka, 1996; Gatome et al., 2010; Mikkonen et al., 1997; Pitkänen & Amaral, 1993; Schmidt et al., 1993; Solodkin et al., 1996; Wouterlood et al., 1995). Meanwhile, in rats, dendrites of large PV+ multipolar layer II-neurons have been shown to reach all the way into layer VI (Wouterlood et al., 1995). Also, small multipolar PV+ neurons have been reported in EC-layer II in humans and non-human primates (Mikkonen et al., 1997; Pitkänen & Amaral, 1993; Schmidt et al., 1993; Tuñón et al., 1992), while they are absent from layer II of rats (Wouterlood et al., 1995).

Note that in addition to providing local innervation, work on rats showed that occasional PV+ neurons provide long-range hippocampal projections, terminating on neurons in stratum lacunosum moleculare of the CA fields and in the molecular layer of the dentate gyrus (Melzer et al., 2012). This finding was recently corroborated with PV+ neurons being shown to provide a speed modulating signal onto hippocampal networks (Ye, Witter, Moser, & Moser, 2018)

5.4.2 | Neuropil

In EC-layer II of humans and monkeys, labelled neuropil, putatively constituting axons, is present within the clusters of stellate cells characteristic of this layer. Such labelling increases until it becomes very dense close to the rhinal/collateral sulcus (Beall & Lewis, 1992; Mikkonen et al., 1997; Schmidt et al., 1993; Tuñón et al., 1992). Topologically, similar labelling is apparent in rodents (Beed et al., 2013; Fujimaru & Kosaka, 1996; Wouterlood et al., 1995).

The terminal distribution of PV+ axons around the somata of principal cells (Hendry et al., 1989), reminiscent of a woven basket, is what gave rise to the name "parvalbumin basket cells." In human, monkey and rat EC, PV+ chandelier-like terminals are also found in layer II (Arellano, DeFelipe, & Munoz, 2002; Pitkänen & Amaral, 1993; Wouterlood et al., 1995). In the case of humans and monkeys, these latter terminals confine to the easily recognizable stellate cell clusters, and in contrast to the preferred termination pattern of basket cells, the terminations of PV+ chandelier cells form radially oriented clusters of terminals, mimicking a chandelier like orientation, specifically targeting the axon initial segment of principal neurons (DeFelipe, Hendry, & Jones, 1989; for further details, see Howard, Tamas, & Soltesz, 2005; Freund & Katona, 2007).

5.5 | Cholecystokinin (CCK+)

5.5.1 | Neurons

Available morphological data on CCK+ neurons are mainly from work in rats and guinea pigs, although sparse data are available in humans. The majority of CCK+ neurons in EC-layer II are of the multipolar type, while vertically oriented CCK+ neurons of the bipolar type are also present (Figure 2e; Köhler & Chan-Palay, 1982; Lotstra & Vanderhaeghen, 1987a,1987b). In human EC-layer II, CCK+ neuropil resembling axon terminals are seen associated with stellate cell clusters, along with what appears to be large beaded fibres with a vertical orientation (Lotstra & Vanderhaeghen, 1987a). In infants, vertically oriented bipolar CCK+ neurons can clearly be seen emitting long beaded processes (Lotstra & Vanderhaeghen, 1987b). In rats and the guinea pig, the overall labelling of CCK + -neuropil increases at levels successively further away from the rhinal sulcus (Figure 2e; Köhler & Chan-Palay, 1982).
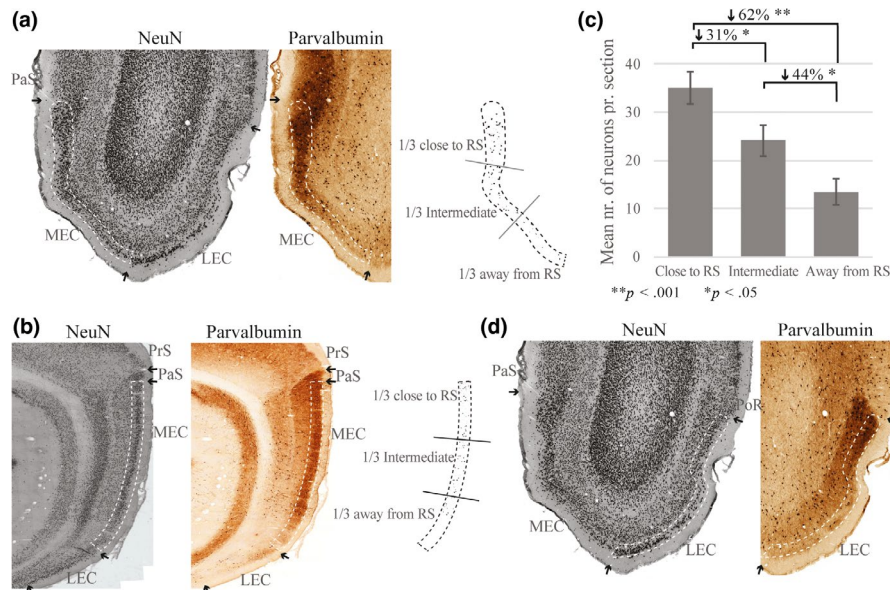
FIGURE 5 Densities of parvalbumin positive (PV+) neurons along the medial entorhinal cortex (MEC)-layer II dorsoventral axis. (a,b) Left to right: delineation of MEC-layer II on a NeuN-stained coronal (a) and sagittal (b) section; the same delineation overlaid on a PV+ labelled adjacent section; 8-bit greyscale converted image of layer II of the PV+ labelled section, on which the domain corresponding to the 1/3 closest to the rhinal sulcus (RS), the domain corresponding to the intermediate 1/3 and the domain corresponding to the 1/3 furthest away from the RS is delimited. For each of the immunolabelled sections used (sections taken from three animals), we applied the same procedure. The delineated MEC-layer II was divided into three, equal-surface domains. The particle analyser tool in ImageJ was calibrated to count cell profiles in the grayscale images, and the mean number of PV+ cell profiles pr. domain pr. section was calculated. (c) The cell profile counts of the sagittal and coronal sections combined revealed a significant 44% drop in the domain corresponding to the 1/3 furthest away from RS compared with the intermediate 1/3, a significant 62% drop in the domain corresponding to the 1/3 furthest away from RS compared with the domain corresponding to the 1/3 closest to RS, and a significant 31% drop in the intermediate 1/3 compared with the domain corresponding to the 1/3 closest to RS. (d) Lateral entorhinal cortex (LEC): Examples of NeuN-stained coronal sections (left for each panel) where layer II has been delineated, followed by adjacent PV+ labelled sections (right for each panel). A substantially higher density of somata appears in the domain close to RS than in the domain located away from RS. Of the coronal sections, those from one of the animals were provided courtesy of Grethe Mari Olsen. Note that data involving the parietal cortex from these sections have previously been published (Olsen & Witter, 2016). Additional coronal as well as the sagittal sections used here have previously been used to show cyto- and chemoarchitectural features of the hippocampal formation and parahippocampal region, published in Kjonigsen et al. (2011) for the coronal sections and in Boccara et al. (2015) for the sagittal sections. All sections are based on immunoperoxidase-labelling. [Colour figure can be viewed at wileyonlinelibrary.com]

5.6 | Somatostatin (SOM+)

5.6.1 | Neurons

Work on humans, monkeys and rats shows that EC-layer II contains SOM+ multipolar and bipolar neurons (Figure 2f; Köhler & Chan-Palay, 1983; Bakst et al., 1985; Chan-Palay, 1987; Carboni et al., 1990). No consistent gradient involving SOM+ appears to be present, although a few apparently species-specific features are notable. For example, in the case of rats, a substantial population of small oval or round SOM+ neurons are present in the portion located furthest away from the rhinal sulcus, and this is more notable for LEC than MEC (Köhler & Chan-Palay, 1983). In monkeys, the density of SOM+ neurons appears highest in the domains located furthest away from the rhinal sulcus (Bakst et al., 1985), but this has not been described in humans (Chan-Palay, 1987).

5.6.2 | Neuropil

SOM+ varicose processes are present in layer II of rats, showing an even distribution throughout the subfields (Köhler & Chan-Palay, 1983). Data from monkeys indicate that such labelling is present at a higher density in the domains located away from the rhinal sulcus (Bakst et al., 1985). In humans, a moderate and non-graded amount of neuropil labelling was described (Chan-Palay, 1987). However, another study indicated that the pattern of such neuropil labelling in humans is similar to that reported for monkeys (Friederich-Ecsy et al., 1988; Figure 2f).

5.7 | Neuropeptide Y (NPY+)

5.7.1 | Neurons

In layer II of humans and monkeys, NPY+ neurons are present in low-to-moderate numbers and consist of small bipolar and to

a lesser extent multipolar types (Chan-Palay, Köhler, Haesler, Lang, & Yasargil, 1986; Köhler, Eriksson, Davies, & Chan-Palay, 1986; Lotstra, Schiffmann, & Vanderhaeghen, 1989). In rats, very few NPY+ neurons reside in layer II; those present are mainly situated in the domain of LEC located furthest away from the rhinal sulcus and consist of large multipolar or bipolar neurons (Figure 2g; Köhler et al., 1986; Köhler, Eriksson, Davies, & Chan-Palay, 1987).

5.7.2 | Neuropil

In all three species, a dense network of NPY+ neuropil is present in layer II. In humans and monkeys, such neuropil surrounds stellate-cell clusters and likely constitutes axons (Chan-Palay et al., 1986; Köhler et al., 1986). In rats, a higher density of such neuropil appears at levels located successively further away from the rhinal sulcus (Köhler et al., 1986).

Aside from the markers discussed above, recent work on mice (Surmeli et al., 2015) and rats (Ohara et al., 2018) shows a subset of neurons in layer II of both MEC and LEC expressing the transcription factor Ctip2.

5.8 | Co-localization

Non-phosphorylated neurofilament proteins containing the *high* and *medium* molecular weight-type subunits being recognized by the monoclonal antibody SMI-32 (SMI-32+) are present in the somatas of a population of neurons in layer II of human and monkey EC (Beall & Lewis, 1991, 1992; Lavenex, Lavenex, Bennett, & Amaral, 2009). The morphology and distribution of SMI-32+ neurons resemble that of RE+ neurons. Specifically, increasing numbers of SMI-32+ neurons are present in domains located successively closer to the rhinal/collateral sulcus (Beall & Lewis, 1992; Lavenex et al., 2009), which is reminiscent of the situation for RE+ neurons. SMI-32+ neurons are also present in EC of rats (Kirkcaldie et al., 2002), and in Wahlberg's epauletted fruit bat, but not in the straw coloured fruit bat (Gatome et al., 2010). Likewise, the Australian echidna (Hassiotis, Paxinos, & Ashwell, 2004, 2005) and Tamar wallaby (Ashwell, Zhang, & Marotte, 2005) show no SMI-32 + labelling in EC. Meanwhile, work in mice shows that the low molecular weight-type subunit of neurofilament proteins is present in putative perforant path-axons from superficial layers (Paulussen, Jacobs, Van der Gucht, Hof, & Arckens, 2011). Whether these axons have their origin in neurons of both layer II and layer III remains to be established.

Recent work on rat MEC shows that a subpopulation of RE+ neurons are enwrapped by perineuronal nets as revealed by labelling with WFA. Moreover, in the portion of MEC located close to the rhinal sulcus, 28% of WFA-labelled neurons are RE+. Moving successively further away from the rhinal sulcus this overlap decreases, until few if any

WFA-labelled neurons are RE+ at the point furthest away from the rhinal sulcus (Lensjø, Christensen, Tennoe, Fyhn, & Hafting, 2017). Perineuronal nets are also present around neurons in superficial layers of human EC (Lendvai et al., 2013; Pantazopoulos, Woo, Lim, Lange, & Berretta, 2010), while the neurochemical identity of these cells remains to be explored.

In rats, a population of neurons in superficial layers of LEC stain positive for enkephalin (Gall, Brecha, Karten, & Chang, 1981). Judging by their distance from the pia, and the fact that enkephalin+ fibres were lost from the outer molecular layer of the dentate gyrus following lesions of LEC (Gall et al., 1981), many of the enkephalin+ neurons are part of the population of RE+ layer II-neurons (Figure 2a). Note that superficial LEC-layer III (possibly including parts of what is alternatively called layer IIb) also contains enkephalin+ neurons (see section on layer III for details). Enkephalin appears absent from principal neurons in MEC (Gall et al., 1981).

In humans, multiple nicotinic acetylcholine receptor subunits, including the α3, α4, α7, β2 and β4 subunits, have a particularly strong expression in neurons residing in the so-called cell islands, also referred to as the pre-alpha neurons. These thus likely represent mainly the RE+ layer II-neurons (Graham et al., 2003). A subset of neurons in these cell-islands are also positive for neuronal NOS (Egberongbe et al., 1994).

Work on EC-layer II in rodents (Kitamura et al., 2014) shows that CB+ neurons to a large extent co-stain with wolfram syndrome 1 protein (Wfs1; Figure 2b). However, it remains to be established whether the co-localization of CB+ and Wfs1 in layer II (or the rest of the layers) is consistent throughout EC. Also, it is conceivable that at least a subset of the SOM+ neurons in EC-layer II are part of the CB+ population (Rogers, 1992). In broad terms, descriptions of the distribution of SOM+ neurons vs CB+ neurons are in line with this notion. We consider the possibility of this latter co-expression further in the case of layer III, where more information is available on such neurons.

Regarding CR+ layer II-neurons, there are notable discrepancies in the literature regarding their neurotransmitter content, as we also point for such neurons in layer I. Work on both rats (Miettinen et al., 1997) and monkeys (Pothuizen et al., 2004) indicates that a large majority of CR+ layer II neurons are GABA+. However, another study reported that only 1/3 of the CR+ neurons are GABA+ in this layer (Wouterlood et al., 2000). As suggested for the comparable discrepancy in layer I, the different findings are likely the result of methodological differences. On the whole, we consider it likely that a majority of CR+ layer II neurons are GABA+.

The majority of CR+ neurons in EC of the rat stain positive for VIP (Rogers, 1992). It is therefore possible if not likely that neurons co-expressing, these markers are

present in layer II. In line with this, the overall morphology and distribution of VIP+ neurons in EC-layer II (and III) of rats (Köhler & Chan-Palay, 1983; Loren et al., 1979) is reminiscent of that described for the CR+ bipolar neurons in this layer (Miettinen et al., 1997; Wouterlood et al., 2000). However, VIP+ neurons in EC-layer II tend to form small clusters (Köhler & Chan-Palay, 1983), which is less notable in the case of CR+ neurons (Miettinen et al., 1997), suggesting that a potential overlap between VIP+ neurons and CR+ neurons is less than complete. A subset of CR+ neurons are weakly positive for the substance P receptor NK$_1$R (Wolansky, Pagliardini, Greer, & Dickson, 2007). The latter author further reported that approximately 1/3 of SST+ and NPY+ neurons in layer II express NK$_1$R+ and that NK$_1$R+ is present in a subset of CB+ neurons in layer II of LEC.

The majority of PV+ neurons in layer II (and III) of MEC label positive for WFA, at least in the case of rats and mice (Lensjø et al., 2017). Whether a similar situation holds true for LEC remains to be explored. Most, if not all PV+ neurons in layer II (as well as in layers III-VI) express m2AChR (Chaudhuri et al., 2005). Furthermore, work on humans and monkeys shows that PV+ terminals selectively stain positive for polysialylated neural cell adhesion molecule (PSA-NCAM) as well as the GABA transporter 1 (GAT1+; DeFelipe et al., 1989; DeFelipe & Gonzalez-Albo, 1998; Arellano et al., 2002).

PSA-NCAM is also expressed by a minor population of neurons in layer II in LEC of rats. These neurons typically have an immature morphology, although some display pyramidal-like morphologies (Foley et al., 2008; Fox et al., 2000; Gomez-Climent et al., 2008). Similar findings were reported for cats (Varea et al., 2011). PSA-NCAM is also present in layer II-neurons of human EC (Murray et al., 2016, 2018; Varea et al., 2007), where its presence is limited to GAD+ neurons co-labelling with either CB+, CR+ or PV+, typically of a small bi-or multipolar morphology (Murray et al., 2016, 2018).

In rat MEC, axons of CCK+ neurons form basket-like pericellular innervations of subgroups of layer II neurons, separated by non-innervated neurons (Köhler, 1986). More recent work revealed that CB+ neurons in MEC are selectively innervated by terminals that stain positive for vesicular glutamate transporter type 3 (VGLUT3; Varga et al., 2010), a transporter present in a subset of CCK+ somata along with CCK+ terminals, at least in rat hippocampus (Somogyi et al., 2004). In addition, *high expression* of cannabinoid receptor type 1 (CB1) was found selectively present in CCK+ neurons in mouse cortex (Marsicano & Lutz, 1999). Labelling with VGLUT3 is therefore thought to selectively provide visualization of the axon terminals of interneurons positive for both CCK and CB1 also in the case of EC, and these neurons are hence referred to as "cholecystokinin and cannabinoid type 1 basket cells" (CCKBCs; Freund & Katona, 2007; Varga et al., 2010). Although *high expression* of CB1 is selectively present in CCK+ neurons, we do not currently know how many CCK+ neurons actually express CB1 in the case of EC. Of further relevance to CCKBCs is their association with the 5-hydroxytryptamine 3A (5HT3A) receptor. Specifically, in MEC layer-II, 5HT3A receptor-expressing neurons and CCKBCs both preferentially target CB+ pyramidal neurons while avoiding RE+ stellate cells (Fuchs et al., 2016). Furthermore, it has been known for some time that in the neocortex, a large majority of CCK+ neurons expresses the 5HT3A receptor, while this receptor is not expressed by either PV+ or SOM+ neurons (Lee, Hjerling-Leffler, Zagha, Fishell, & Rudy, 2010; Morales & Bloom, 1997). Recently, a dissociation between PV+, SOM+ and 5HT3A receptor-expressing neurons was also shown in EC (Fuchs et al., 2016). Thus, in EC, as in the neocortex, immunolabelling against CCK likely targets the 5HT3A receptor-expressing population of neurons with a high degree of selectivity.

Of the large multipolar or bipolar NPY+ neurons in ventral LEC, a large proportion (up to 89%) co-stain for somatostatin (Figure 2g; Köhler et al., 1986, 1987).

Layer II-neurons in rats express high levels of 5HT1a receptor-mRNA (Chalmers & Watson, 1991; Hammer, Hori, Blanchard, & Blanchard, 1992). Meanwhile, labelling with antibodies against the 5HT1a receptor indicates its presence throughout the layers (Chalmers & Watson, 1991; Hammer et al., 1992). Based on autoradiographic analysis of selective ligand binding, this is also the case in guinea pigs (Sijbesma, Schipper, Cornelissen, & Dekloet, 1991) and humans (Barone, Jordan, Atger, Kopp, & Fillion, 1994; Pazos, Probst, & Palacios, 1987), and for the latter, it is evident that the highest levels of receptor binding are present rostrally and laterally, that is, towards the collateral sulcus (Pazos et al., 1987). Interestingly, work on rats shows that while all layers in EC are innervated by 5-HT-positive fibres originating in the raphe nuclei, particularly dense patches of such fibres are located in layer II towards the rhinal sulcus (Köhler, Chan-Palay, Haglund, & Steinbusch, 1980; Köhler, Chan-Palay, & Steinbusch, 1981). These patches likely arise from neurons in the ipsilateral dorsal raphe nucleus (Köhler & Steinbusch, 1982).

5.9 | Conclusions, layer II

In layer II across species, several neuroanatomical markers selectively label unique subsets of neuronal populations, such that a large majority of layer II neurons can be accounted for by the selective markers currently available. Furthermore, we emphasize that certain markers remain to be tested outside of rodents, with one notable example being enkephalin, of which the expression in LEC-layer II of rats likely labels a subpopulation of RE+ fan neurons.

6 | LAYER III

6.1 | Reelin (RE+)

Many pyramidal neurons in layer III exhibit weak immunoreactivity to reelin across different species (Martinez-Cerdeno et al., 2003; Miettinen et al., 2005; Perez-Garcia et al., 2001; Ramos-Moreno et al., 2006). In addition, small, scattered RE+ interneurons with a multipolar or fusiform morphology are present, along with a low-to-moderate level of RE+ neuropil (Figure 2a; Martinez-Cerdeno et al., 2003; Perez-Garcia et al., 2001; Ramos-Moreno et al., 2006).

6.2 | Calbindin (CB+)

EC-layer III of humans and monkeys contains similar types of CB+ neurons including multipolar, bipolar and pyramidal neurons (Beall & Lewis, 1992; Mikkonen et al., 1997; Suzuki & Porteros, 2002; Tuñón et al., 1992). CB+ multipolar as well as bipolar neurons in layer III have not been reported in rodent EC. However, upon inspection, we do find a sparse population of such neurons in layer III of rats (Figure S2c,d; summarized in Figure 2b). A gradient in CB+ neurons exists in layer III such that the density increases when moving away from the collateral/rhinal sulcus. In humans and monkeys, it has been established that this gradient is most striking for pyramidal neurons, followed by multipolar neurons and bipolar neurons, respectively (Mikkonen et al., 1997; Suzuki & Porteros, 2002), and this is likely also the case for rodents (see below).

Although CB+ expression in layer III in humans and monkeys is highly similar, a few differences exist. As with layer II, the layer III-density of CB+ multipolar neurons is lower in monkeys than in humans (Seress et al., 1994; Suzuki & Porteros, 2002). Although CB+ pyramidal-shaped neurons in both humans and monkeys tend to cluster (Beall & Lewis, 1992), they mainly reside in the superficial half of the layer in humans (Beall & Lewis, 1992; Mikkonen et al., 1997), whereas in monkeys, they appear more evenly distributed throughout the depth of layer III (Seress et al., 1994; Suzuki & Porteros, 2002).

In the rat, it follows from the considerations on layer II (see section on calbindin for layer II) that the question of CB+ pyramidal neurons in layer III will also depend on the scheme for delineation. As described above, according to the original definition of layer III (Cajal, 1901; Lorente de Nó, 1933), CB+ pyramidal neurons are present in the superficial half of layer III in rats (Figures 2b and 3a,c), thus corresponding to that reported for humans. In mice, however, the situation regarding CB+ pyramidal neurons in layer III is more complicated. Essentially, layer III of MEC in mice contain none, or at least very few CB+ pyramidal neurons, irrespective of whether the original or the alternative scheme for

delineation is used (Figure 4c). Meanwhile, in LEC of mice, CB+ pyramidal neurons take up an increasingly deeper position when moving in the direction towards the rhinal sulcus (i.e., dorsolaterally). Thus, following the original definition of layers II/III, the majority of CB+ pyramidal neurons in the portions furthers away from the rhinal sulcus belong to layer II (Figure 4b), whereas those located intermedially and close to the rhinal sulcus belong to layer III (alternatively called layer IIb; Figure 4a). For both rats and mice, CB+ pyramidal neurons tend to cluster and appear to be more numerous in the domains located away from the rhinal sulcus, thus corresponding to that described for monkeys and humans.

6.2.1 | Neuropil

In monkeys, and to a lesser extent in humans, domains located away from the rhinal/collateral sulcus contain dense CB+ labelling throughout layer III. When moving towards the rhinal/collateral sulcus, a label-free zone in the deep part of layer III becomes increasingly apparent, while labelling in the upper two-thirds of the layer becomes less dense (Figure 2b; Mikkonen et al., 1997; Suzuki & Porteros, 2002). Regarding the mouse, a study reported dense neuropil labelling in layer III in LEC, compared with relatively light staining in MEC (Fujimaru & Kosaka, 1996). We observed a similar feature in the rat, where dense CB+ labelling is present both in the superficial and deep half of layer III in LEC, being particularly prominent in the portion located furthest away from the rhinal sulcus, while in layer III of MEC, such labelling is virtually absent in the deep half (Figure S2b).

6.3 | Calretinin (CR+)

6.3.1 | Neurons

Across EC of humans (Brion & Resibois, 1994; Mikkonen et al., 1997), monkeys (Pothuizen et al., 2004; Seress et al., 1993) and rats (Miettinen et al., 1997; Wouterlood et al., 2000) layer III contains the same types of CR+ neurons, which, as with layer II, includes multipolar neurons and bipolar neurons (Figure 2c).

Aside from the small- to medium-sized CR+ neurons reported across species, additional large CR+ multipolar neurons have been observed in layer III of rats. This latter type has obliquely ascending thick dendrites extending up to the pia, in addition to thinner dendrites extending horizontally within the layer or descending into deep layers. Each of these dendritic types give rise to occasional spines on their distal parts. In rat LEC, such large neurons reside superficially within layer III, having somata with a distinct lateral separation of about 500 μm. In contrast, in rat MEC, large CR+ multipolar neurons are less common and reside at various depths with no apparent regularity (Wouterlood et al., 2000). Also in rats,

CR+ bipolar neurons in layer III are particularly numerous in the portion of LEC located furthest away from the rhinal sulcus; available data do not indicate a topologically similar feature in the case of humans or monkeys (Figure 2c).

6.3.2 | Neuropil

Overall, layer III has the strongest CR+ neuropil labelling among the layers. In humans, such labelling follows a clear gradient, with dense labelling in the domains located furthest away from the collateral sulcus and decreasing labelling in domains located successively closer to the collateral sulcus (Mikkonen et al., 1997). A topologically similar feature is present in layer III of rats (Figure 2c; Miettinen et al., 1997; Wouterlood et al., 2000).

6.4 | Parvalbumin (PV+)

Across species, EC-layer III has a similar strong gradient of immunoreactivity to parvalbumin as that described for layer II (see above).

6.4.1 | Neurons

PV+ neurons in layer III are of multipolar and to a lesser extent bipolar morphologies (Figure 2d). Superficial parts of layer III in humans and monkeys contain somata of large and vertically oriented multipolar PV+ neurons. Among these, some align with the classical clusters of stellate cells present in layer II, whereas others situate in alignment with the gaps between the stellate cells and emit processes both into layer I and into deeper layers (Beall & Lewis, 1992; Mikkonen et al., 1997; Solodkin et al., 1996). Regarding the former type, morphologically similar PV+ neurons reside in deep parts of layer II in conjunction with stellate cell clusters, giving the impression that a distinct population of vertically oriented multipolar PV+ neurons traverses layers II and III (Beall & Lewis, 1992). In humans, monkeys and rats, deep parts of layer III also contain large multipolar PV+ neurons. These typically extend dendrites in all directions within their parent layer, along with dendrites of which some ascend into layer I and others descend into layers V and VI (Beall & Lewis, 1992; Mikkonen et al., 1997; Pitkänen & Amaral, 1993; Schmidt et al., 1993; Wouterlood et al., 1995). Yet another type of large multipolar PV+ neuron in deep layer III, exclusively described in humans, has dendrites that extend horizontally within the layer (Schmidt et al., 1993).

PV+ bipolar neurons in layer III of humans appear like those present in layer II. The largest are vertically oriented and have ascending dendrites reaching deep layer II, whereas their descending dendrites rarely pierce layer IV (Schmidt et al., 1993). Although PV+ bipolar neurons have not previously been described in layer III of rodents, we find a sparse presence of such neurons with vertical orientations in rats (Figure S2e).

6.4.2 | Neuropil

In line with the density of somata, the domains located furthest away from the rhinal/collateral sulcus in all species studied contain little PV+ neuropil labelling. Labelling density increases progressively towards intermediate portions and this continues until very dense labelling is present in the domains located closest to the sulcus (Figure 2d; human: Mikkonen et al., 1997; Schmidt et al., 1993; Tuñón et al., 1992; monkey: Pitkänen & Amaral, 1993; rodent: Fujimaru & Kosaka, 1996; Wouterlood et al., 1995). As with layer II, layer III in human, monkey and rat EC also contains short PV+ chandelier-like terminals that are most numerous in superficial parts of the layer (Arellano et al., 2002; Pitkänen & Amaral, 1993; Wouterlood et al., 1995).

6.5 | Cholecystokinin (CCK+)

6.5.1 | Neurons

As summarized in Figure 2e, data from rats and guinea pigs show that EC-layer III contains the same morphological types of CCK+ neurons as those present in layer II, including multipolar and vertically oriented bipolar neurons along with numerous small round or ovoid neurons in the portion of LEC located furthest away from the rhinal sulcus. Additionally, bipolar neurons with distinct, obliquely orientated dendrites have been described in this layer (Köhler & Chan-Palay, 1982)

6.5.2 | Neuropil

In rats and guinea pigs, layer III contains the lowest amount of CCK+ neuropil among the cell layers. Similar to layer II, the overall neuropil labelling in layer III of these species tend to increase at positions successively further away from the rhinal sulcus (Köhler & Chan-Palay, 1982). In humans, vertically oriented CCK+ neuropil that resemble axon terminals are present but we lack data on whether there is a gradient in density (Figure 2e; Lotstra & Vanderhaeghen, 1987a).

6.6 | Somatostatin (SOM+)

6.6.1 | Neurons

SOM+ somata in monkeys and rats are more numerous in the domains located away from the rhinal sulcus (Bakst et al., 1985; Köhler & Chan-Palay, 1983). Meanwhile, the sparse descriptions available for humans do not indicate such a feature

relative to the collateral sulcus (Chan-Palay, 1987). As in layer II, SOM+ neurons in layer III have multipolar and bipolar morphologies (Figure 2f; Bakst et al., 1985; Carboni et al., 1990; Chan-Palay, 1987; Friederich-Ecsy et al., 1988; Köhler & Chan-Palay, 1983). Many of the CCK+ layer III-neurons give rise to very long axons traversing the cortical layers, making up part of the axon terminals seen in layer I (Bakst et al., 1985; Chan-Palay, 1987; Friederich-Ecsy et al., 1988; Tahvildari et al., 2012). This latter type of neuron constitutes Martinotti cells (Tahvildari et al., 2012).

6.6.2 | Neuropil

Overall, SOM+ neuropil labelling within layer III seems to parallel that of the somata in rats, monkeys and humans (Figure 2f; Bakst et al., 1985; Friederich-Ecsy et al., 1988; Köhler & Chan-Palay, 1983), but see Chan-Palay (1987).

6.7 | Neuropeptide Y (NPY+)

6.7.1 | Neurons

NPY+ neurons in EC-layer III of humans, monkeys and rats include bipolar and to a lesser extent multipolar neurons (Chan-Palay et al., 1986; Köhler et al., 1986; Lotstra et al., 1989). In the case of rats, NPY+ neurons appear most numerous in LEC, in particular in the portion of LEC located furthest away from the rhinal sulcus (Figure 2g; Köhler et al., 1986).

6.7.2 | Neuropil

Relatively dense NPY+ neuropil labelling is present in layer III of humans, monkeys and rats. In humans, the somata of layer-III pyramidal neurons appear invested with NPY+ fibre terminals (Chan-Palay et al., 1986). Such a feature is not observed in rats (Köhler et al., 1986), where the overall NPY+ neuropil labelling appears to increase at levels located successively further away from the rhinal sulcus (Köhler et al., 1986), a feature not noted in primates (Figure 2g).

6.8 | Co-localization

In rats, a population of neurons located superficially in EC-layer III (alternatively called layer IIb) in the domain close to the rhinal sulcus labels positive for cyclooxygenase type 2 (COX2+), which is a rate-limiting enzyme in the synthesis of prostanoids and intimately involved in the process of inflammation (Breder, Dewitt, & Kraig, 1995). Considering their morphology and position within the layer, it seems likely that at least part of these COX2+ neurons constitute CB+ pyramidal neurons (Figure 2b). Conversely, moving away from the rhinal sulcus, COX2 appears confined to a

subset of mainly small interneurons. A complete lack of COX2+ dendritic labelling in these latter neurons impairs morphological comparison against known subgroups of interneurons.

In rats, SOM+ neurons follow the same gradient as CB+ bipolar neurons (see above), which is in line with a possible co-localization between these molecules in this particular population of neurons (Rogers, 1992).

As mentioned for layer II (see above), superficial parts of LEC contain a population of neurons that stain positive for enkephalin. While the majority of these belong to layer II and are likely part of the RE+ population, a minority appears situated in superficial layer III (alternatively called IIb; Figure 2b). Indeed, aside from the loss of enkephalin+ neuropil in the outer molecular layer of the dentate gyrus, lesioning LEC also resulted in a loss of such labelling in stratum lacunosum moleculare of CA1, suggesting this constituted labelled axons from EC (Gall et al., 1981). Whether or not these CA1 projecting enkephalin+ neurons co-localize with the sparse population of CB+ neurons that project to CA1 (Kitamura et al., 2014) remains to be established, but this seems likely judging from present data.

The low molecular weight-type subunit of neurofilament proteins (Paulussen et al., 2011) present in putative perforant path axons (see layer II) may take their origin at least in part from layer III-neurons, although we underline that this remains to be established.

Overall, a lower percentage of CR+ neurons in layer III are positive for GABA or GAD than what is the case for layers I and II. In both monkeys and rats, 60% of CR+ neurons in EC-layer III reportedly stain positive for GABA or GAD (Miettinen et al., 1997; Pothuizen et al., 2004). However, another study on rats reported that only 20% of CR+ layer III-neurons are GABA+ (Wouterlood et al., 2000). Notably, the portion of CR+ neurons co-expressing GABA or GAD in layer III of rats appears confined to the superficial half of the layer (Miettinen et al., 1997).

A consideration of potential overlap between CR+ and VIP+ neurons in layer III is relevant, because, as mentioned for both layers I and II, the majority of CR+ neurons in EC stain positive for VIP (Rogers, 1992). In rats, VIP+ neurons in EC-layer III include vertically oriented aspiny bipolar neurons in both LEC and MEC. Furthermore, layer III in LEC also contains multipolar VIP+ neurons that appear aspiny (Köhler & Chan-Palay, 1983). The presence of multipolar VIP+ neurons in layer III of LEC and their absence in MEC are in line with a possible co-localization between VIP+ and CR+ in this layer, as also CR+ neurons of the multipolar type are more common in LEC than in MEC. In addition, as with layer II, VIP+ neurons in LEC-layer III are more numerous in the domains located away from the rhinal sulcus, a feature resembling that reported for CR+ neurons (Köhler & Chan-Palay, 1983).

The majority of PV+ neurons in layer III (as in layer II) of MEC label positive for WFA, at least in the case of rats and mice (Lensjø et al., 2017). Meanwhile, for LEC, this remains to be explored. Regarding the short PV+ chandelier-like terminals present in layer III across species, these selectively label positive for PSA-NCAM and GAT1, at least in humans (Arellano et al., 2002; DeFelipe & Gonzalez-Albo, 1998). Moreover, PSA-NCAM is expressed on the somata of a minor population of layer III-neurons in rats (Foley et al., 2008; Fox et al., 2000; Gomez-Climent et al., 2008), cats (Varea et al., 2011) and humans (Murray et al., 2016, 2018; Varea et al., 2007). As for layer II (see above), work on human EC shows that PSA-NCAM in layer III is selectively present in GAD+ neurons, co-labels with either CB+, CR+ or PV+, and typically associate with neurons having a small bi-or multipolar morphology (Murray et al., 2016, 2018). Also, most, if not all PV+ neurons in layer III (as in the other cell layers) express m2AChR (Chaudhuri et al., 2005).

As in layer II, it is possible that most NPY+ neurons in layer III are also SOM+, judging by data obtained in rats (Köhler et al., 1987).

In rats, neurons in all layers in EC express the 5HT1a-receptor and are innervated by 5-HT-positive fibres originating in the raphe nuclei. However, a particularly dense network of such fibres distribute in layer III of LEC (Köhler et al., 1980, 1981) and likely arise from neurons in the ipsilateral dorsal raphe nucleus (Köhler & Steinbusch, 1982). As suggested by these authors, this indicates that the raphe nuclei can selectively modulate LEC circuits.

6.9 | Conclusions, layer III

Taken together, the currently available selective neuroanatomical markers cover most if not all neuronal populations in EC-layer III, as is the case with layer II (see above). Importantly, the various markers to a very high degree label the same morphological types of neurons across species.

7 | LAYER IV (LAMINA DISSECANS)

Although layer IV is often referred to as an acellular layer, neurons are present albeit in low numbers. Current knowledge of neuroanatomical markers present in layer IV is summarized in Figure 2a–g.

8 | LAYER V

8.1 | Reelin (RE+)

Sparse data from studies on ferrets and rats suggest that small, scattered RE+ bi- and multipolar neurons along with sparse

neuropil-labelling are present in layer V (Martinez-Cerdeno et al., 2003; Ramos-Moreno et al., 2006; own unpublished data).

8.2 | Calbindin (CB+)

8.2.1 | Neurons

In humans, monkeys and rats, relatively few CB+ neurons are present in layer V as compared with layers II and III (Figure 2b). Those present in layer V include multipolar and bipolar neurons that are mostly of small to medium size, although a low number of large multipolar CB+ neurons also reside here. In contrast to layers II and III, there is no clear gradient related to position with respect to the rhinal/collateral sulcus (Mikkonen et al., 1997; Seress et al., 1994; Suzuki & Porteros, 2002). However, the olfactory field of EC in the monkey appears to constitute an exception to the otherwise homogenous layer V labelling, as relatively high numbers of CB+ neurons reside here, even including a sparse population of pyramidal neurons (Suzuki & Porteros, 2002).

8.2.2 | Neuropil

In monkeys, CB+ neuropil labelling in layer V is relatively light in rostral portions. Meanwhile, contrasting the CB+ labelling present in somata and dendrites in this layer, putative axon labelling increases at increasingly more caudal positions, such that the caudal and caudal limiting subfields of the monkey EC contain a fairly strong band of such putative CB+ axons (Suzuki & Porteros, 2002). This feature appears less obvious in humans (Figure 2b; Mikkonen et al., 1997). As for rats, the moderately dense band of labelled neuropil present in layer IV (see section on calbindin for layer IV above) seems to extend into superficial parts of layer V.

8.3 | Calretinin (CR+)

8.3.1 | Neurons

In humans, monkeys, rats and the domestic pig, layer V contains multipolar, bipolar and putative pyramidal CR+ neurons (Figure 2c; Chaudhuri et al., 2005; Miettinen et al., 1997; Mikkonen et al., 1997, 1999; Pothuizen et al., 2004). In humans, the latter type is darkly labelled and mainly resides in rostral and medial portions, that is, away from the collateral sulcus. The pyramidal-like morphology of these neurons is obvious in that it includes two primary basal dendrites descending obliquely towards layer VI while giving off thinner secondary branches, and one thick primary apical dendrite ascending into layer III with little apparent branching (Mikkonen et al., 1997, 1999). Similar findings were reported for both monkeys (Pothuizen et al., 2004) and rats

(Chaudhuri et al., 2005; Miettinen et al., 1997), although here such neurons appear less intensely labelled.

8.3.2 | Neuropil

CR+ neuropil labelling in human EC-layer V parallels the density of CR+ somata in this layer, such that dense labelling is present in the domains located away from the collateral sulcus, while labelling gradually decreases when moving successively closer to the collateral sulcus (Mikkonen et al., 1997, 1999). A topologically comparable pattern is present in rats (Figure 2c; Miettinen et al., 1997).

8.4 | Parvalbumin (PV+)

As with the other cell layers, EC-layer V of humans, monkeys and rodents contains PV+ neurons that are most numerous towards the rhinal/collateral sulcus (Figure 2d; Fujimaru & Kosaka, 1996; Mikkonen et al., 1997; Pitkänen & Amaral, 1993; Wouterlood et al., 1995).

8.4.1 | Neurons

As in the superficial layers, PV+ neurons in layer V are comparable across species and consist of multipolar and bipolar types (Figure 2d), although again, a few differences are notable. For example, while large-sized multipolar PV+ neurons are common in layer V of humans and monkeys (Mikkonen et al., 1997; Pitkänen & Amaral, 1993; Schmidt et al., 1993; Solodkin et al., 1996; Tuñón et al., 1992), such neurons are sparse in layer V of rats ((Wouterlood et al., 1995); own unpublished observations). PV+ bipolar neurons are also common in layer V in humans and monkeys (Mikkonen et al., 1997; Pitkänen & Amaral, 1993; Schmidt et al., 1993), contrasting with the relative paucity of such neurons in layer V of rats (Wouterlood et al., 1995; own unpublished observations). Among the medium to large bipolar neurons described in layer V in humans is a unique type emitting conspicuously bent and varicose dendrites. This type of bipolar neuron has been shown to emit axons giving rise to cartridges that correspond to those of chandelier cells (Schmidt et al., 1993).

8.4.2 | Neuropil

In humans and monkeys, PV+ neuropil labelling in layer V appears to align with the overall neuronal PV+ labelling (Figure 2d). Thus, such labelling is weak in the domains located furthest away from the rhinal/collateral sulcus, while gradually increasing until dense labelling is present in the domains located close to the rhinal/collateral sulcus (Mikkonen et al., 1997; Pitkänen & Amaral, 1993; Schmidt et al., 1993; Tuñón et al., 1992). A topologically comparable

situation appears evident in rodents (Fujimaru & Kosaka, 1996; Wouterlood et al., 1995).

8.5 | Cholecystokinin (CCK+)

8.5.1 | Neurons

Several different morphological types of CCK+ neurons are present in EC-layer V of rodents (Figure 2e). Such neurons include small horizontally oriented (presumably bipolar) neurons that are particularly numerous medially in MEC, occasional pyramidal-like neurons, small multipolar neurons and unipolar neurons. While no information is currently available on the dendritic extent of these neurons, their axons can occasionally be followed down to the white matter (Köhler & Chan-Palay, 1982; Phan, 2015), likely targeting various cortical areas including auditory cortex (Li et al., 2014). Regarding humans, the sparse data available suggest that occasional CCK+ neurons are present in layer V, while no morphological detail is available (Lotstra & Vanderhaeghen, 1987b; Savasta, Palacios, & Mengod, 1990).

8.5.2 | Neuropil

Overall, CCK+ neuropil-labelling in the rat is relatively dense in the portions located away from the rhinal sulcus (Köhler & Chan-Palay, 1982). Labelled neuropil is also present in humans in this layer, showing a beaded appearance and vertical orientations (Lotstra & Vanderhaeghen, 1987a,1987b).

8.6 | Somatostatin (SOM+)

8.6.1 | Neurons

Data on SOM+ neurons are available from humans, monkeys and rats. Overall, SOM+ neurons are more numerous in deep layers than in superficial layers of EC. In layer V, such neurons have bipolar and multipolar morphologies (Figure 2f; Bakst et al., 1985; Carboni et al., 1990; Chan-Palay, 1987; Friederich-Ecsy et al., 1988; Wouterlood & Pothuizen, 2000), and, in the case of rats, pyramidal morphologies (Köhler & Chan-Palay, 1983). Of the SOM+ neurons in humans and monkeys, some emit very long axons that traverse the cortical layers, likely making up part of the axon terminals seen in layer I (Bakst et al., 1985; Carboni et al., 1990; Chan-Palay, 1987; Friederich-Ecsy et al., 1988); such neurons likely constitute Martinotti cells.

8.6.2 | Neuropil

In rats, SOM+ neuropil labelling is very dense in the superficial half of layer V (Köhler & Chan-Palay, 1983). In monkeys, labelled neuropil appear strongest in the domains located away from the rhinal sulcus, most notably in deep

parts of the layer, where labelled neuropil with both horizontal and radial orientations are present. In middle and superficial parts of layer V, such neuropil are mainly radially oriented (Bakst et al., 1985). A similar pattern has been suggested to be present in humans (Figure 2f; Friederich-Ecsy et al., 1988), although note that another study on humans did not find such a gradient (Chan-Palay, 1987).

8.7 | Neuropeptide Y (NPY+)

8.7.1 | Neurons

In EC of humans, monkeys and rats, NPY+ neurons are more numerous in layer V than in superficial layers (Figure 2g). In EC-layer V of rats, NPY+ neurons appear to mainly constitute medium sized horizontally oriented bipolar neurons (Köhler et al., 1986), whereas for humans and monkeys, NPY+ neurons more commonly include multipolar neurons (Chan-Palay et al., 1986; Köhler et al., 1986; Lotstra et al., 1989). In the case of rats, similar to that described for superficial layers, NPY+ neurons are most numerous in the portion of LEC located furthest away from the rhinal sulcus (Köhler et al., 1987).

8.7.2 | Neuropil

A dense NPY+ plexus of neuropil is present in layer V in humans (Chan-Palay et al., 1986; Lotstra et al., 1989). This is less notable in monkeys and rats (Köhler et al., 1986).

Recently, two novel neuroanatomical markers were found to label separate populations of neurons restricted to the classically (based on cytoarchitecture) defined superficial (layer Va) vs deep (layer Vb) part of layer V. Specifically, work in mice demonstrated that the transcription factor Etv1 is expressed in layer Va, while the transcription factor-interacting protein Ctip2 is expressed in layer Vb (Ramsden, Surmeli, McDonagh, & Nolan, 2015; Surmeli et al., 2015). This molecular split between layers Va vs Vb also holds true in rats (Ohara et al., 2018) and potentially opens new avenues into selective manipulations of the circuits to which neurons in these sublayers belong.

8.8 | Co-localization

In monkeys and rats, about 15% of CR+ neurons label positive for GABA. In both species, the large CR+ neurons that are likely to constitute pyramidal neurons (see above) belong to the majority of EC layer V-neurons that are negative for GABA (Miettinen et al., 1997; Pothuizen et al., 2004; Wouterlood et al., 2000). Meanwhile, the reported high overlap between CR+ neurons and VIP+ neurons in EC of rats (Rogers, 1992) may also include neurons in layer V. From the sparse data available, VIP+ neurons in layer V appear to

include bipolar neurons and horizontally oriented multipolar neurons with short aspiny dendrites (Köhler & Chan-Palay, 1983), which is in line with such a potential co-expression, at least for a subset of these neurons.

In rats, a subset of CR+ neurons in layer V are weakly positive for NK_1R (Wolansky et al., 2007). Also among the NPY+ neurons in layer V, a subset express NK_1R (Wolansky et al., 2007), and it is likely that some NPY+ neurons also express somatostatin (Köhler et al., 1987).

Most, if not all PV+ neurons in layer V (as in the other cell layers) express m2AChR (Chaudhuri et al., 2005). In monkeys, occasional neurons in this layer express mRNA for preprogalanin (Evans, Huntley, Morrison, Shine, & Paxinos, 1992). In humans, neuronal NOS appears to be present in a substantial proportion of pyramidal and multipolar neurons (Egberongbe et al., 1994; Katsuse, Iseki, & Kosaka, 2003; Sobreviela & Mufson, 1995; Yew, Wong, Li, Lai, & Yu, 1999).

8.9 | Conclusions, layer V

With respect to neuroanatomical markers, like that of the cytoarchitecture, what emerges for layer V across species is homology. While dense PV+ labelling characterizes the domains close to the rhinal/collateral sulcus, a loss of PV+ labelling and an increasing presence of CR+ neurons with pyramidal morphologies indicates the domains further away from the rhinal/collateral sulcus. Meanwhile, recent work additionally enables the molecular separation of superficial (Etv1) vs deep (ctip2) layer V-neurons in rodents, while such a potential separation in humans and non-human primates awaits further study.

9 | LAYER VI

9.1 | Reelin (RE+)

No detailed description of RE+ neurons is available for layer VI. Based on the sparse information available for rats and ferrets, this layer appears to contain a small population of RE+ bipolar and multipolar neurons (Martinez-Cerdeno et al., 2003; Ramos-Moreno et al., 2006). Like in layer V, a low level of neuropil-labelling is present in layer VI (Martinez-Cerdeno et al., 2003; own unpublished observations).

9.2 | Calbindin (CB+)

9.2.1 | Neurons

In humans, monkeys and rats, EC-layer VI contains the same morphological types of CB+ neurons as those reported for layer V (Figure 2b), including small- to medium-sized bipolar neurons and multipolar neurons of varying sizes (Figure S2c,d; Mikkonen et al., 1997, 1999; Seress et al., 1994;

Suzuki & Porteros, 2002). In humans, large CB+ multipolar layer VI-neurons have labelled dendrites descending into layer V (Mikkonen et al., 1997). In the rat, we observed a clear difference with respect to the number of CB+ neurons in LEC vs MEC. Whereas LEC contains a relatively high number of CB+ neurons, such neurons are very sparse in MEC (Figure S2f).

9.2.2 | Neuropil

In humans and monkeys, the overall CB+ neuropil labelling in EC-layer VI is very low, with slightly higher levels rostrally than caudally (Mikkonen et al., 1997; Suzuki & Porteros, 2002). EC-layer VI in mice also contains a low level of labelled neuropil (Fujimaru & Kosaka, 1996), while in the rat, we observe slightly higher levels in LEC than in MEC (Figure S2f).

9.3 | Calretinin (CR+)

9.3.1 | Neurons

Work on humans, monkeys and rats show that similar to layer V, layer VI contains large CR+ neurons. In humans, such neurons frequently have a pyramidal-like morphology with apical dendrites descending into layer III (Mikkonen et al., 1997). Meanwhile, the morphology of such large CR+ neurons remains to be established for monkeys and rats, but is seems a likely inference that at least part of them are of the pyramidal type. In humans and monkeys, such large CR+ neurons are numerous in the domains located furthest away from the rhinal/collateral sulcus (Figure 2c), where they are located throughout the depth of the layer. Moving gradually towards the CS, such neurons take up a superficial position within layer VI, at which point they appear as a single band stretching across the layer when viewed under low power magnification. Meanwhile, the domains located closest to the rhinal/collateral sulcus contain few such neurons (Mikkonen et al., 1997, 1999; Pothuizen et al., 2004). In addition, EC-layer VI of all three species contains bipolar neurons and small- to medium-sized spherical multipolar neurons positive for calretinin (Miettinen et al., 1997; Mikkonen et al., 1997; Pothuizen et al., 2004; Seress et al., 1993; Wouterlood et al., 2000).

9.3.2 | Neuropil

CR+ neuropil labelling in layer VI of humans is similar to that described for layer V, thus following a gradient where the domains furthest away from the collateral sulcus are heavily labelled, while the domains located closer to the collateral sulcus contain progressively less labelling (Mikkonen et al., 1997, 1999). A topologically similar, though less obvious gradient of CR+ neuropil labelling appears to be present also in rats (Figure 2c; Miettinen et al., 1997).

9.4 | Parvalbumin (PV+)

9.4.1 | Neurons

In layer VI of humans, monkeys and rats, PV+ neurons are predominantly present in the domains located towards the collateral/rhinal sulcus (Figure 2d; Mikkonen et al., 1997; Pitkänen & Amaral, 1993; Wouterlood et al., 1995). PV+ multipolar neurons ranging from small to medium in size have been described in this layer in humans (Mikkonen et al., 1997; Schmidt et al., 1993; Tuñón et al., 1992) and rats (Wouterlood et al., 1995). PV+ bipolar neurons are also present (Mikkonen et al., 1997; Pitkänen & Amaral, 1993; Schmidt et al., 1993; own unpublished observation), and work on humans shows that of the ones with a small or medium size soma, some emit conspicuously varicose dendrites together with axons that form chandelier-like cartridges (Schmidt et al., 1993).

9.4.2 | Neuropil

Layer VI in humans and monkeys contain sparse PV+ neuropil labelling, except at the portions closest to the rhinal/collateral sulcus where moderate labelling is visible (Mikkonen et al., 1997; Pitkänen & Amaral, 1993). In rodents, topologically similar labelling appears to be present (Fujimaru & Kosaka, 1996; Wouterlood et al., 1995).

9.5 | Cholecystokinin (CCK+)

Work on rats shows that EC-layer VI contain neurons with fusiform as well as ovoid CCK+ somata. Such neurons are of both bipolar and multipolar types (Figure 2e), often emitting relatively long and oblique or horizontally oriented primary dendrites from which secondary dendrites descend into layer V. A low density of CCK+ neuropil is present, with no apparent gradient (Köhler & Chan-Palay, 1982). As with layer V, information on layer VI CCK+ neurons in humans is largely missing, though a low density of such neurons appears present. Furthermore, beaded neuropil of mostly vertical orientation is present in layer VI of humans (Lotstra & Vanderhaeghen, 1987a,1987b).

9.6 | Somatostatin (SOM+)

SOM+ neurons in EC-layer VI of humans, monkeys and rats have small to medium sized round or oval somata, including both multipolar and bipolar neurons (Carboni et al., 1990; Friederich-Ecsy et al., 1988; Köhler & Chan-Palay, 1983; Wouterlood & Pothuizen, 2000). In monkeys, bipolar SOM+

neurons are typically vertically oriented (Carboni et al., 1990). In layer VI of rat LEC, numerous labelled neurons are present in the domain located furthest away from the rhinal sulcus; this is similar to that of layers II, III and V (Figure 2f). Regarding neuropil, a moderate amount of labelling is present in rats (Köhler & Chan-Palay, 1983), while this seems low in the case of monkeys (Bakst et al., 1985) and humans (Friederich-Ecsy et al., 1988).

9.7 | Neuropeptide Y (NPY+)

9.7.1 | Neurons

In EC-layer VI of humans, monkeys and rats, NPY+ neurons are abundant as compared with either of the superficial layers, and NPY-labelling reveals the same morphological types of neurons as those present in layer V (Figure 2g). In rat MEC, NPY+ neurons in layer VI are predominantly of the horizontally oriented bipolar type, whereas for LEC, which contains a higher density of somata, multipolar neurons are also common (Köhler et al., 1986). Similar to layers II, III and V, layer VI in rats contains the highest density of NPY+ neurons in the domains of LEC located furthest away from the rhinal sulcus (Köhler et al., 1986). In layer VI of humans (Chan-Palay et al., 1986; Lotstra et al., 1989) and monkeys (Köhler et al., 1986), medium-sized multipolar neurons appear to predominate. Deep in layer VI in humans, at and across the border to the white matter, large bipolar as well as multipolar NPY+ neurons reside (Chan-Palay et al., 1986).

9.7.2 | Neuropil

In humans, monkeys and rats, immunolabelling against NPY reveals a moderate to high density of neuropil in EC-layer VI. The superficial one-third of layer VI appears to contain more labelling than middle and deep parts, at least in humans (Chan-Palay et al., 1986; Köhler et al., 1986, 1987; Lotstra et al., 1989).

9.8 | Co-localization

Only a low percentage of the CR+ neurons in EC-layer VI are likely GABAergic. In rats, the percentage of CR+ neurons in EC-layer VI that label positive for GABA or GAD was estimated to be 13% by one study (Wouterlood et al., 2000), and 24% by another study (Miettinen et al., 1997). Meanwhile, in layer VI of monkeys, about 9% of such neurons label positive for GABA (Pothuizen et al., 2004).

As pointed out for layers I–V, most CR+ neurons in EC of rats label positive for VIP, although the study in question did not provide details concerning individual layers (Rogers, 1992). As with layer V, VIP+ neurons in layer VI are sparsely present and include neurons with diverse morphologies (Köhler & Chan-Palay, 1983). However, detailed information on the

morphological characteristics of VIP+ neurons in EC-layer VI is currently not available, preventing a comparison with CR+ neurons in this layer. Meanwhile, a portion of the NPY+ neurons likely co-express somatostatin (Chan-Palay, 1987).

Most, if not all PV+ neurons in layer VI (as in the other cell layers) express m2AChR (Chaudhuri et al., 2005). As with layer V, data in monkeys show that a few neurons in layer VI express mRNA for preprogalanin (Evans et al., 1992). In humans, neuronal NOS appears to be present in a substantial population of neurons (Katsuse et al., 2003; Sobreviela & Mufson, 1995; Yew et al., 1999).

9.9 | Conclusions layer VI

Across species, the situation in layer VI reflects that reported for the other layers, meaning several neuroanatomical markers label the same basic cell types. Furthermore, as with the adjoining layer V, dense PV+ labelling characterizes the domains close to the rhinal/collateral sulcus also in layer VI, while a loss of PV+ labelling and an increasing presence of CR+ neurons with pyramidal morphologies indicate the domains further away from the rhinal/collateral sulcus.

10 | FUNCTIONALLY DIFFERENT POPULATIONS DISCERNIBLE BY NEUROANATOMICAL MARKERS

Findings in rodents suggest that superficial layers of EC contain at least three populations of interneurons that are separable by way of immunolabelling against parvalbumin, somatostatin and cholecystokinin, with the latter population also expressing the 5HT3A receptor (from here on referred to as CCK/5HT3A+ neurons). These particular molecular constituents likely relate to a functional division, as the three populations make contact with distinct groups of principal neurons.

The increasing presence of PV+ neurons towards the rhinal sulcus (in rodents and monkeys) or collateral sulcus (in humans) coincides with reelin levels in layer II principal neurons (Kobro-Flatmoen et al., 2016; Perez-Garcia et al., 2001). Furthermore, work on rodents has established that the majority of RE+ principal neurons in MEC-layer II constitute stellate cells and form the sole MEC layer II-projection onto the dentate gyrus (Fuchs et al., 2016; Kitamura et al., 2014; Varga et al., 2010). In LEC-layer II, reelin is present in all morphological types of principal neurons, including all fan neurons, but only part of the multipolar and pyramidal populations. Like in MEC, all RE+ neurons in LEC give rise to the projection onto the dentate gyrus (Leitner et al., 2016). Electrophysiological recordings in rodents from the domain of MEC adjacent to the rhinal sulcus revealed that stellate cells are interconnected via

fast-spiking interneurons (Couey et al., 2013; Fuchs et al., 2016; Pastoll et al., 2013) that are likely identical with the PV+ neurons (Beed et al., 2013). Taken together, these lines of evidence strongly suggest that PV+ interneurons target RE+ principal neurons along a gradient, such that the degree to which the latter are under inhibitory control by PV+ neurons gradually increases in domains located progressively closer to the rhinal/collateral sulcus. Cortical PV+ neurons, driven by local principal neurons, permit the type of rapid computations that enable crucial aspects of our cognitive capacities (Freund & Katona, 2007). Observations in rat MEC revealed graded differences in the resolution of spatial coding, with grid cells located close to the rhinal sulcus having fine-grained spatial representations, and grid cells located successively further away from the rhinal sulcus having successively more coarse-grained spatial representations (Brun et al., 2008; Stensola et al., 2012). This is interesting in view of the present neuroanatomical data, as being under a stronger inhibitory control by PV+ neurons may be interpreted as an indication that RE+ neurons in MEC-layer II located close to the rhinal sulcus are capable of forming more precise representations than such neurons located further away from the rhinal sulcus. Given the similar anatomical relationship in LEC-layer II, one might expect a comparable situation with the most fine-grained representations being present close to the rhinal sulcus.

In rodents, the target cells in layer II for CCK/5HT3A+ neurons mainly are CB+ principal neurons, most of which have a pyramidal morphology (Fuchs et al., 2016; Varga et al., 2010). In the hippocampus, serotonergic projections from the median raphe nucleus were shown to target CCK/5HT3A+ neurons (Freund, 2003), but avoiding PV+ neurons (Freund, Gulyas, Acsady, Gorcs, & Toth, 1990; Papp, Hajos, Acsady, & Freund, 1999). This serotonergic targeting of CCK/5HT3A+ neurons has been proposed to underlie fear-related information processing (Freund, 2003; Freund & Katona, 2007). In this context, fundamental observations are the anxiolytic effects provided by serotonin antagonists (Jones et al., 1988) and the treatment efficacy of selective serotonin reuptake inhibitors in mood disorders (Kent, Coplan, & Gorman, 1998). In addition, the anxiolytic benzodiazepines act selectively on α-2-subunit-containing GABAA receptors (Low et al., 2000), which are enriched at hippocampal synapses formed where CCK+ interneurons target pyramidal neurons (Nyíri, Freund, & Somogyi, 2001). Notably, as for the hippocampus, the raphe nuclei provide prominent innervation onto EC (Köhler & Steinbusch, 1982); however, whether serotonergic raphe-projections selectively target CCK/5HT3A+ neurons in EC remains to be explored. Such data would further a functional understanding of both CCK/5HT3A+ neurons and their CB+ target-neurons in EC.

Recent work on the connectivity-profile of entorhinal SOM+ interneurons revealed yet another remarkable degree of interneuron-to-principal neuron selectivity. Thus, SOM+ neurons located superficially in mouse MEC contact both RE+ stellate cells and intermediate pyramidal neurons, but avoid CB+ pyramidal neurons and intermediate stellate cells (Fuchs et al., 2016). In addition, SOM+ interneurons (putative Martinotti cells) situated in deeper layers likely constitute an additional source of interneuron-input onto superficially located principal neurons. Future work should reveal whether these latter interneurons exhibit selectivity for any specific neuronal population(s). Interestingly, hippocampal somatostatin signalling has been linked to the selection of memory strategies, in that activation of the somatostatin-type 4 receptor appears involved in switching from engagement of the spatial memory system to the cue-based dorsal striatal system (Gastambide, Viollet, Lepousez, Epelbaum, & Guillou, 2009; Gastambide et al., 2010). Whether somatostatin in EC contributes to this remains to be explored.

A fairly new approach in the field of neuroscience is single-cell sequencing of a neurons' transcriptome. This offers a powerful tool to interrogate neuronal heterogeneity in defined systems, such as that underway in the hippocampus proper where novel classes of inhibitory neurons were recently demonstrated (Harris et al., 2018), or to probe molecular signatures across developmental stages as recently done on proliferating cells in the dentate gyrus (Hochgerner, Zeisel, Lonnerberg, & Linnarsson, 2018). Also, for the cytoarchitecturally more complex EC, it is highly likely that the application of single-cell sequencing will uncover a greater molecular heterogeneity among neurons than what our current understanding amounts to.

11 | CONCLUDING REMARKS

The available cross-species neuroanatomical data on EC clearly indicate that along with its phylogenetically highly conserved cytoarchitecture there is also a highly conserved chemoarchitecture. Uncovering these relationships allows for testable predictions, for example the prediction developed above that that RE+ neurons in EC-layer II located close to the rhinal sulcus likely form more precise representations of coded information than such neurons located further away from the rhinal sulcus. Moreover, as we have shown in this review, a comparable chemoarchitecture for similar cell types is present across species, and thus the same basic functional relationship may hold true as well. Intriguingly, we recently provided evidence that RE+ principal neurons in an AD rat model, specifically those located close to the rhinal sulcus, are selectively vulnerable to AD-associated accumulation of intracellular amyloid-β (Kobro-Flatmoen et al., 2016), which fits with current evidence that early

Alzheimer-related symptoms typically involve deficits in fine-grained recall (Dubois et al., 2014). The uncovering of grid cells in both monkeys (Killian, Jutras, & Buffalo, 2012) and humans (Jacobs et al., 2013), actualizes the question of whether graded differences in the resolution of spatial coding in primates fall along the axis comparable to that of rodents, namely with increasing spatial granularity towards the rhinal/collateral sulcus. If so, this will further underline the utility of rodent models to interrogate both the healthy and the diseased EC, anchored to a continuing effort to develop a thorough understanding of the underlying anatomy.

ACKNOWLEDGEMENTS

CONFLICTS OF INTEREST

The authors declare that they have no conflict of interests/competing financial interests.

AUTHOR CONTRIBUTIONS

AK-F and MPW wrote the paper together and AK-F did the data analysis.

ORCID

Asgeir Kobro-Flatmoen (iD) https://orcid.org/0000-0002-2379-2982

Menno P. Witter (iD) https://orcid.org/0000-0003-0285-1637

REFERENCES

Abraham, H., Toth, Z., & Seress, L. (2004). A novel population of calretinin-positive neurons comprises reelin-positive Cajal-Retzius cells in the hippocampal formation of the adult domestic pig. *Hippocampus*, *14*, 385–401.

Alcantara, S., Ruiz, M., D'Arcangelo, G., Ezan, F., de Lecea, L., Curran, T., … Soriano, E. (1998). Regional and cellular patterns of reelin mRNA expression in the forebrain of the developing and adult mouse. *Journal of Neuroscience*, *18*, 7779–7799.

Amaral, D. G., Insausti, R., & Cowan, W. M. (1987). The entorhinal cortex of the monkey: I. Cytoarchitectonic organization. *Journal of Comparative Neurology*, *264*, 326–355.

Arellano, J. I., DeFelipe, J., & Munoz, A. (2002). PSA-NCAM immunoreactivity in chandelier cell axon terminals of the human temporal cortex. *Cerebral Cortex*, *12*, 617–624.

Ashwell, K. W., Zhang, L. L., & Marotte, L. R. (2005). Cyto- and chemoarchitecture of the cortex of the tammar wallaby (*Macropus eugenii*): Areal organization. *Brain, Behavior and Evolution*, *66*, 114–136.

Bakst, I., Morrison, J. H., & Amaral, D. G. (1985). The distribution of somatostatin-like immunoreactivity in the monkey hippocampal formation. *Journal of Comparative Neurology*, *236*, 423–442.

Barone, P., Jordan, D., Atger, F., Kopp, N., & Fillion, G. (1994). Quantitative autoradiography of 5-HT1D and 5-HT1E binding sites labelled by [3H]5-HT, in frontal cortex and the hippocampal region of the human brain. *Brain Research*, *638*, 85–94.

Beall, M. J., & Lewis, D. A. (1991). Comparison of the intrinsic organization of monkey and human entorhinal cortex. *Society for Neuroscience Abstracts*, *17*, 128. (Abstract).

Beall, M. J., & Lewis, D. A. (1992). Heterogeneity of layer II neurons in human entorhinal cortex. *Journal of Comparative Neurology*, *321*, 241–266.

Beed, P., Gundlfinger, A., Schneiderbauer, S., Song, J., Bohm, C., Burgalossi, A., … Schmitz, D. (2013). Inhibitory gradient along the dorsoventral axis in the medial entorhinal cortex. *Neuron*, *79*, 1197–1207.

Berger, B., De Grissac, N., & Alvarez, C. (1999). Precocious development of parvalbumin-like immunoreactive interneurons in the hippocampal formation and entorhinal cortex of the fetal cynomolgus monkey. *Journal of Comparative Neurology*, *403*, 309–331.

Blackstad, T. W. (1956). Commissural connections of the hippocampal region in the rat, with special reference to their mode of termination. *Journal of Comparative Neurology*, *105*, 417–537.

Boccara, C. N., Kjonigsen, L. J., Hammer, I. M., Bjaalie, J. G., Leergaard, T. B., & Witter, M. P. (2015). A three-plane architectonic atlas of the rat hippocampal region. *Hippocampus*, *25*, 838–857.

Breder, C. D., Dewitt, D., & Kraig, R. P. (1995). Characterization of inducible cyclooxygenase in rat brain. *Journal of Comparative Neurology*, *355*, 296–315.

Brion, J. P., & Resibois, A. (1994). A subset of calretinin-positive neurons are abnormal in Alzheimer's disease. *Acta Neuropathologica*, *88*, 33–43.

Brun, V. H., Solstad, T., Kjelstrup, K. B., Fyhn, M., Witter, M. P., Moser, E. I., & Moser, M. B. (2008). Progressive increase in grid scale from dorsal to ventral medial entorhinal cortex. *Hippocampus*, *18*, 1200–1212.

Cajal, S. R. Y. (1901). Estudios sobre la corteza cerebral humana: IV. Estructura de la corteza cerebral olfativa del hombre y mamíferos. *Trabajos Laboratory Investigation Biology of Madrid*, *1*, 1–140.

Canto, C. B. (2011). *Layer specific integrative properties of entorhinal principal neurons*. Thesis. Norwegian University of Science and Technology Trondheim, Norway. ISBN 978-82-471-2962-3.

Canto, C. B., Wouterlood, F. G., & Witter, M. P. (2008). What does the anatomical organization of the entorhinal cortex tell us? *Neural Plasticity*, *2008*, 381243.

Cappaert, N. L. M., Van Strien, N. M., & Witter, M. P. (2015). Hippocampal formation. In G. Paxinos (Ed.), *The rat nervous system* (pp. 511–574). San Diego, CA; London, UK: Elsevier Academic Press.

Carboni, A. A., Lavelle, W. G., Barnes, C. L., & Cipolloni, P. B. (1990). Neurons of the lateral entorhinal cortex of the rhesus monkey: A Golgi, histochemical, and immunocytochemical characterization. *Journal of Comparative Neurology*, *291*, 583–608.

Celio, M. R. (1990). Calbindin D-28k and parvalbumin in the rat nervous system. *Neuroscience*, *35*, 375–475.

Chalmers, D. T., & Watson, S. J. (1991). Comparative anatomical distribution of 5-HT1A receptor mRNA and 5-HT1A binding in rat brain

– a combined in situ hybridisation/in vitro receptor autoradiographic study. *Brain Research*, *561*, 51–60.

Chan-Palay, V. (1987). Somatostatin immunoreactive neurons in the human hippocampus and cortex shown by immunogold/silver intensification on vibratome sections: coexistence with neuropeptide Y neurons, and effects in Alzheimer-type dementia. *Journal of Comparative Neurology*, *260*, 201–223.

Chan-Palay, V., Köhler, C., Haesler, U., Lang, W., & Yasargil, G. (1986). Distribution of neurons and axons immunoreactive with antisera against neuropeptide Y in the normal human hippocampus. *Journal of Comparative Neurology*, *248*, 360–375.

Chaudhuri, J. D., Hiltunen, M., Nykanen, M., Yla-Herttuala, S., Soininen, H., & Miettinen, R. (2005). Localization of M2 muscarinic receptor protein in parvalbumin and calretinin containing cells of the adult rat entorhinal cortex using two complementary methods. *Neuroscience*, *131*, 557–566.

Couey, J. J., Witoelar, A., Zhang, S. J., Zheng, K., Ye, J., Dunn, B., … Witter, M. P. (2013). Recurrent inhibitory circuitry as a mechanism for grid formation. *Nature Neuroscience*, *16*, 318–324.

DeFelipe, J., & Gonzalez-Albo, M. C. (1998). Chandelier cell axons are immunoreactive for GAT-1 in the human neocortex. *NeuroReport*, *9*, 467–470.

DeFelipe, J., Hendry, S. H., & Jones, E. G. (1989). Visualization of chandelier cell axons by parvalbumin immunoreactivity in monkey cerebral cortex. *Proceedings of the National Academy of Sciences of the United States of America*, *86*, 2093–2097.

DeFelipe, J., Lopez-Cruz, P. L., Benavides-Piccione, R., Bielza, C., Larranaga, P., Anderson, S., … Ascoli, G. A. (2013). New insights into the classification and nomenclature of cortical GABAergic interneurons. *Nature Reviews Neuroscience*, *14*, 202–216.

Deshmukh, S. S., & Knierim, J. J. (2011). Representation of non-spatial and spatial information in the lateral entorhinal cortex. *Frontiers in Behavioural Neurosciences*, *5*, 69.

Drakew, A., Frotscher, M., Deller, T., Ogawa, M., & Heimrich, B. (1998). Developmental distribution of a reeler gene-related antigen in the rat hippocampal formation visualized by CR-50 immunocytochemistry. *Neuroscience*, *82*, 1079–1086.

Dubois, B., Feldman, H. H., Jacova, C., Hampel, H., Molinuevo, J. L., Blennow, K., … Cummings, J. L. (2014). Advancing research diagnostic criteria for Alzheimer's disease: the IWG-2 criteria. *Lancet Neurology*, *13*, 614–629.

von, Economo, C. (2009). *Cellular structure of the human cerebral cortex (translated and edited by L. C. Triarhou)*. Thessaloniki, Greece: Karger.

Egberongbe, Y. I., Gentleman, S. M., Falkai, P., Bogerts, B., Polak, J. M., & Roberts, G. W. (1994). The distribution of nitric oxide synthase immunoreactivity in the human brain. *Neuroscience*, *59*, 561–578.

Evans, H. F., Huntley, G. W., Morrison, J. H., Shine, J., & Paxinos, G. (1992). Localization of preprogalanin mRNA in the monkey hippocampal formation. *Neuroscience Letters*, *146*, 171–175.

Ferrer, I., Zujar, M. J., Admella, C., & Alcantara, S. (1992). Parvalbumin and calbindin immunoreactivity in the cerebral cortex of the hedgehog (*Erinaceus europaeus*). *Journal of Anatomy*, *180*, 165–174.

Foley, A. G., Hirst, W. D., Gallagher, H. C., Barry, C., Hagan, J. J., Upton, N., … Regan, C. M. (2008). The selective 5-HT6 receptor antagonists SB-271046 and SB-399885 potentiate NCAM PSA immunolabeling of dentate granule cells, but not neurogenesis, in the hippocampal formation of mature Wistar rats. *Neuropharmacology*, *54*, 1166–1174.

Fox, G. B., Fichera, G., Barry, T., O'Connell, A. W., Gallagher, H. C., Murphy, K. J., & Regan, C. M. (2000). Consolidation of passive avoidance learning is associated with transient increases of polysialylated neurons in layer II of the rat medial temporal cortex. *Journal of Neurobiology*, *45*, 135–141.

Freund, T. F. (2003). Interneuron diversity series: Rhythm and mood in perisomatic inhibition. *Trends in Neurosciences*, *26*, 489–495.

Freund, T. F., Gulyas, A. I., Acsady, L., Gorcs, T., & Toth, K. (1990). Serotonergic control of the hippocampus via local inhibitory interneurons. *Proceedings of the National Academy of Sciences of the United States of America*, *87*, 8501–8505.

Freund, T. F., & Katona, I. (2007). Perisomatic inhibition. *Neuron*, *56*, 33–42.

Friederich-Ecsy, B., Braak, E., Braak, H., & Probst, A. (1988). Somatostatin-like immunoreactivity in non-pyramidal neurons of the human entorhinal region. *Cell and Tissue Research*, *254*, 361–367.

Fuchs, E. C., Neitz, A., Pinna, R., Melzer, S., Caputi, A., & Monyer, H. (2016). Local and distant input controlling excitation in layer II of the medial entorhinal cortex. *Neuron*, *89*, 194–208.

Fujimaru, Y., & Kosaka, T. (1996). The distribution of two calcium binding proteins, calbindin D-28K and parvalbumin, in the entorhinal cortex of the adult mouse. *Neuroscience Research*, *24*, 329–343.

Fyhn, M., Molden, S., Witter, M. P., Moser, E. I., & Moser, M. B. (2004). Spatial representation in the entorhinal cortex. *Science*, *305*, 1258–1264.

Gall, C., Brecha, N., Karten, H. J., & Chang, K. J. (1981). Localization of enkephalin-like immunoreactivity to identified axonal and neuronal populations of the rat hippocampus. *Journal of Comparative Neurology*, *198*, 335–350.

Gastambide, F., Lepousez, G., Viollet, C., Loudes, C., Epelbaum, J., & Guillou, J. L. (2010). Cooperation between hippocampal somatostatin receptor subtypes 4 and 2: functional relevance in interactive memory systems. *Hippocampus*, *20*, 745–757.

Gastambide, F., Viollet, C., Lepousez, G., Epelbaum, J., & Guillou, J. L. (2009). Hippocampal SSTR4 somatostatin receptors control the selection of memory strategies. *Psychopharmacology (Berl)*, *202*, 153–163.

Gatome, C. W., Slomianka, L., Mwangi, D. K., Lipp, H. P., & Amrein, I. (2010). The entorhinal cortex of the Megachiroptera: a comparative study of Wahlberg's epauletted fruit bat and the straw-coloured fruit bat. *Brain Structure and Function*, *214*, 375–393.

Gomez-Climent, M. A., Castillo-Gomez, E., Varea, E., Guirado, R., Blasco-Ibanez, J. M., Crespo, C., … Nacher, J. (2008). A population of prenatally generated cells in the rat paleocortex maintains an immature neuronal phenotype into adulthood. *Cerebral Cortex*, *18*, 2229–2240.

Graham, A. J., Ray, M. A., Perry, E. K., Jaros, E., Perry, R. H., Volsen, S. G., … Court, J. A. (2003). Differential nicotinic acetylcholine receptor subunit expression in the human hippocampus. *Journal of Chemical Neuroanatomy*, *25*, 97–113.

van Groen, T., Miettinen, P., & Kadish, I. (2003). The entorhinal cortex of the mouse: Organization of the projection to the hippocampal formation. *Hippocampus*, *13*, 133–149.

Hammer, R. P. Jr, Hori, K. M., Blanchard, R. J., & Blanchard, D. C. (1992). Domestication alters 5-HT1A receptor binding in rat brain. *Pharmacology, Biochemistry and Behavior*, *42*, 25–28.

Harris, K.D., Hochgerner, H., Skene, N.G., Magno, L., Katona, L., Bengtsson Gonzales, C., … Hjerling-Leffler, J. (2018) Classes and

continua of hippocampal CA1 inhibitory neurons revealed by single-cell transcriptomics. *PLoS Biol.*, 16, e2006387.

Hassiotis, M., Paxinos, G., & Ashwell, K. W. (2004). Cyto- and chemoarchitecture of the cerebral cortex of the Australian echidna (Tachyglossus aculeatus). I. Areal organization. *Journal of Comparative Neurology*, 475, 493–517.

Hassiotis, M., Paxinos, G., & Ashwell, K. W. (2005). Cyto- and chemoarchitecture of the cerebral cortex of an echidna (*Tachyglossus aculeatus*). II. Laminar organization and synaptic density. *Journal of Comparative Neurology*, 482, 94–122.

Hendry, S. H., Jones, E. G., Emson, P. C., Lawson, D. E., Heizmann, C. W., & Streit, P. (1989). Two classes of cortical GABA neurons defined by differential calcium binding protein immunoreactivities. *Experimental Brain Research*, 76, 467–472.

Herring, A., Donath, A., Steiner, K. M., Widera, M. P., Hamzehian, S., Kanakis, D., … Keyvani, K. (2012). Reelin depletion is an early phenomenon of Alzheimer's pathology. *Journal of Alzheimer's Disease*, 30, 963–979.

Hochgerner, H., Zeisel, A., Lonnerberg, P., & Linnarsson, S. (2018). Conserved properties of dentate gyrus neurogenesis across postnatal development revealed by single-cell RNA sequencing. *Nature Neuroscience*, 21, 290–299.

Howard, A., Tamas, G., & Soltesz, I. (2005). Lighting the chandelier: new vistas for axo-axonic cells. *Trends in Neurosciences*, 28, 310–316.

Insausti, R. (1993). Comparative anatomy of the entorhinal cortex and hippocampus in mammals. *Hippocampus*, 3, 19–26.

Insausti, R., & Amaral, D. G. (2008). Entorhinal cortex of the monkey: IV. Topographical and laminar organization of cortical afferents. *Journal of Comparative Neurology*, 509, 608–641.

Insausti, R., & Amaral, D. G. (2012). Hippocampal formation. In K. M. Juergen, & G. Paxinos (Eds.), *The human nervous system* (pp. 896–942). London, UK: Academic Press.

Insausti, R., Herrero, M. T., & Witter, M. P. (1997). Entorhinal cortex of the rat: Cytoarchitectonic subdivisions and the origin and distribution of cortical efferents. *Hippocampus*, 7, 146–183.

Insausti, R., Munoz-Lopez, M., Insausti, A. M., & Artacho-Perula, E. (2017). The human periallocortex: layer pattern in presubiculum, parasubiculum and entorhinal cortex. A review. *Frontiers in Neuroanatomy*, 11, 84.

Insausti, R., Tuñón, T., Sobreviela, T., Insausti, A. M., & Gonzalo, L. M. (1995). The human entorhinal cortex: A cytoarchitectonic analysis. *Journal of Comparative Neurology*, 355, 171–198.

Jacobs, J., Weidemann, C. T., Miller, J. F., Solway, A., Burke, J. F., Wei, X. X., … Kahana, M. J. (2013). Direct recordings of grid-like neuronal activity in human spatial navigation. *Nature Neuroscience*, 16, 1188–1190.

Jones, B. J., Costall, B., Domeney, A. M., Kelly, M. E., Naylor, R. J., Oakley, N. R., & Tyers, M. B. (1988). The potential anxiolytic activity of GR38032F, a 5-HT3-receptor antagonist. *British Journal of Pharmacology*, 93, 985–993.

Katsuse, O., Iseki, E., & Kosaka, K. (2003). Immunohistochemical study of the expression of cytokines and nitric oxide synthases in brains of patients with dementia with Lewy bodies. *Neuropathology*, 23, 9–15.

Kent, J. M., Coplan, J. D., & Gorman, J. M. (1998). Clinical utility of the selective serotonin reuptake inhibitors in the spectrum of anxiety. *Biological Psychiatry*, 44, 812–824.

Killian, N. J., Jutras, M. J., & Buffalo, E. A. (2012). A map of visual space in the primate entorhinal cortex. *Nature*, 491, 761–764.

Kirkcaldie, M. T., Dickson, T. C., King, C. E., Grasby, D., Riederer, B. M., & Vickers, J. C. (2002). Neurofilament triplet proteins are restricted to a subset of neurons in the rat neocortex. *Journal of Chemical Neuroanatomy*, 24, 163–171.

Kitamura, T., Pignatelli, M., Suh, J., Kohara, K., Yoshiki, A., Abe, K., & Tonegawa, S. (2014). Island cells control temporal association memory. *Science*, 343, 896–901.

Kjonigsen, L. J., Leergaard, T. B., Witter, M. P., & Bjaalie, J. G. (2011). Digital atlas of anatomical subdivisions and boundaries of the rat hippocampal region. *Frontiers in Neuroinformatics*, 5, 2.

Klausberger, T., & Somogyi, P. (2008). Neuronal diversity and temporal dynamics: the unity of hippocampal circuit operations. *Science*, 321, 53–57.

Kleven, H., Gatome, W., Las, L., Ulanovsky, N., & Witter, M. P. (2014). *Organization of entorhinal-hippocampal projections in the Egyptian fruit bat Federation of European Neuroscience Societies*. Milano, Italy: FENS, Abstract 3642.

Kobayashi and Amaral (1999). Chemical neuroanatomy of the hippocampal formation and the perirhinal and parahippocampal cortices. In F. E. Bloom, A. Björklund, & T. Hökfelt (Eds.), *Handbook of chemical neuroanatomy* (pp. 378–388). Amsterdam, the Netherlands: Elsevier Science.

Kobro-Flatmoen, A., Nagelhus, A., & Witter, M. P. (2016). Reelin-immunoreactive neurons in entorhinal cortex layer II selectively express intracellular amyloid in early Alzheimer's disease. *Neurobiology of Diseases*, 93, 172–183.

Köhler, C. (1986). Cytochemical architecture of the entorhinal area. *Advances in Experimental Medicine and Biology*, 203, 83–98.

Köhler, C., & Chan-Palay, V. (1982). The distribution of cholecystokinin-like immunoreactive neurons and nerve terminals in the retrohippocampal region in the rat and guinea pig. *Journal of Comparative Neurology*, 210, 136–146.

Köhler, C., & Chan-Palay, V. (1983). Somatostatin and vasoactive intestinal polypeptide-like immunoreactive cells and terminals in the retrohippocampal region of the rat brain. *Anatomy and Embryology (Berlin)*, 167, 151–172.

Köhler, C., Chan-Palay, V., Haglund, L., & Steinbusch, H. (1980). Immunohistochemical localization of serotonin nerve terminals in the lateral entorhinal cortex of the rat: Demonstration of two separate patterns of innervation from the midbrain raphe. *Anatomy and Embryology (Berlin)*, 160, 121–129.

Köhler, C., Chan-Palay, V., & Steinbusch, H. (1981). The distribution and orientation of serotonin fibers in the entorhinal and other retrohippocampal areas. An immunohistochemical study with anti-serotonin antibodies in the rats brain. *Anatomy and Embryology (Berlin)*, 161, 237–264.

Köhler, C., Eriksson, L., Davies, S., & Chan-Palay, V. (1986). Neuropeptide Y innervation of the hippocampal region in the rat and monkey brain. *Journal of Comparative Neurology*, 244, 384–400.

Köhler, C., Eriksson, L. G., Davies, S., & Chan-Palay, V. (1987). Colocalization of neuropeptide tyrosine and somatostatin immunoreactivity in neurons of individual subfields of the rat hippocampal region. *Neuroscience Letters*, 78, 1–6.

Köhler, C., & Steinbusch, H. (1982). Identification of serotonin and non-serotonin-containing neurons of the mid-brain raphe projecting to the entorhinal area and the hippocampal formation. A combined

immunohistochemical and fluorescent retrograde tracing study in the rat brain. *Neuroscience*, 7, 951–975.

Krimer, L. S., Hyde, T. M., Herman, M. M., & Saunders, R. C. (1997). The entorhinal cortex: An examination of cyto- and myeloarchitectonic organization in humans. *Cerebral Cortex*, 7, 722–731.

Kropff, E., Carmichael, J. E., Moser, M. B., & Moser, E. I. (2015). Speed cells in the medial entorhinal cortex. *Nature*, 523, 419–424.

Lavenex, P., Lavenex, P. B., Bennett, J. L., & Amaral, D. G. (2009). Postmortem changes in the neuroanatomical characteristics of the primate brain: hippocampal formation. *Journal of Comparative Neurology*, 512, 27–51.

Lee, S., Hjerling-Leffler, J., Zagha, E., Fishell, G., & Rudy, B. (2010). The largest group of superficial neocortical GABAergic interneurons expresses ionotropic serotonin receptors. *Journal of Neuroscience*, 30, 16796–16808.

Leitner, F. C., Melzer, S., Lutcke, H., Pinna, R., Seeburg, P. H., Helmchen, F., & Monyer, H. (2016). Spatially segregated feedforward and feedback neurons support differential odor processing in the lateral entorhinal cortex. *Nature Neuroscience*, 19, 935–944.

Lendvai, D., Morawski, M., Negyessy, L., Gati, G., Jager, C., Baksa, G., … Alpar, A. (2013). Neurochemical mapping of the human hippocampus reveals perisynaptic matrix around functional synapses in Alzheimer's disease. *Acta Neuropathologica*, 125, 215–229.

Lensjø, K. K., Christensen, A. C., Tennoe, S., Fyhn, M., & Hafting, T. (2017). Differential expression and cell-type specificity of perineuronal nets in hippocampus, medial entorhinal cortex, and visual cortex examined in the rat and mouse. *eNeuro*, 4, 1–18. https://doi.org/10.1523/eneuro.0379-16.2017

Lerner, T. N., Ye, L., & Deisseroth, K. (2016). Communication in neural circuits: Tools, opportunities, and challenges. *Cell*, 164, 1136–1150.

Li, X., Yu, K., Zhang, Z., Sun, W., Yang, Z., Feng, J., … He, J. (2014). Cholecystokinin from the entorhinal cortex enables neural plasticity in the auditory cortex. *Cell Research*, 24, 307–330.

Loren, I., Emson, P. C., Fahrenkrug, J., Bjorklund, A., Alumets, J., Hakanson, R., & Sundler, F. (1979). Distribution of vasoactive intestinal polypeptide in the rat and mouse brain. *Neuroscience*, 4, 1953–1976.

Lorente de Nó, R. (1933). Studies on the structure of the cerebral cortex. *Journal of Psychology and Neurology*, 45, 381–438.

Lotstra, F., Schiffmann, S. N., & Vanderhaeghen, J. J. (1989). Neuropeptide Y-containing neurons in the human infant hippocampus. *Brain Research*, 478, 211–226.

Lotstra, F., & Vanderhaeghen, J. J. (1987a). Distribution of immunoreactive cholecystokinin in the human hippocampus. *Peptides*, 8, 911–920.

Lotstra, F., & Vanderhaeghen, J. J. (1987b). High concentration of cholecystokinin neurons in the newborn human entorhinal cortex. *Neuroscience Letters*, 80, 191–196.

Low, K., Crestani, F., Keist, R., Benke, D., Brunig, I., Benson, J. A., … Rudolph, U. (2000). Molecular and neuronal substrate for the selective attenuation of anxiety. *Science*, 290, 131–134.

Luo, L., Callaway, E. M., & Svoboda, K. (2008). Genetic dissection of neural circuits. *Neuron*, 57, 634–660.

Lykken, C., & Kentros, C. G. (2014). Beyond the bolus: Transgenic tools for investigating the neurophysiology of learning and memory. *Learning and Memory*, 21, 506–518.

Maass, A., Berron, D., Libby, L. A., Ranganath, C., & Duzel, E. (2015). Functional subregions of the human entorhinal cortex. *Elife*, 4, e06426.

Markram, H., Toledo-Rodriguez, M., Wang, Y., Gupta, A., Silberberg, G., & Wu, C. (2004). Interneurons of the neocortical inhibitory system. *Nature Reviews Neuroscience*, 5, 793–807.

Marsicano, G., & Lutz, B. (1999). Expression of the cannabinoid receptor CB1 in distinct neuronal subpopulations in the adult mouse forebrain. *European Journal of Neuroscience*, 11, 4213–4225.

Martínez-Cerdeño, V., Galazo, M. J., Cavada, C., & Clascá, F. (2002). Reelin immunoreactivity in the adult primate brain: Intracellular localization in projecting and local circuit neurons of the cerebral cortex, hippocampus and subcortical regions. *Cerebral Cortex*, 12, 1298–1311.

Martinez-Cerdeno, V., Galazo, M. J., & Clasca, F. (2003). Reelin-immunoreactive neurons, axons, and neuropil in the adult ferret brain: Evidence for axonal secretion of reelin in long axonal pathways. *Journal of Comparative Neurology*, 463, 92–116.

Melzer, S., Michael, M., Caputi, A., Eliava, M., Fuchs, E. C., Whittington, M. A., & Monyer, H. (2012). Long-range-projecting GABAergic neurons modulate inhibition in hippocampus and entorhinal cortex. *Science*, 335, 1506–1510.

Miettinen, M., Koivisto, E., Riekkinen, P., & Miettinen, R. (1996). Coexistence of parvalbumin and GABA in nonpyramidal neurons of the rat entorhinal cortex. *Brain Research*, 706, 113–122.

Miettinen, M., Pitkänen, A., & Miettinen, R. (1997). Distribution of calretinin-immunoreactivity in the rat entorhinal cortex: Coexistence with GABA. *Journal of Comparative Neurology*, 378, 363–378.

Miettinen, R., Riedel, A., Kalesnykas, G., Kettunen, H. P., Puolivali, J., Soininen, H., & Arendt, T. (2005). Reelin-immunoreactivity in the hippocampal formation of 9-month-old wildtype mouse: Effects of APP/PS1 genotype and ovariectomy. *Journal of Chemical Neuroanatomy*, 30, 105–118.

Miettinen, R., Sirvio, J., Riekkinen, P. Sr, Laakso, M. P., Riekkinen, M., & Riekkinen, P. Jr (1993). Neocortical, hippocampal and septal parvalbumin- and somatostatin-containing neurons in young and aged rats: Correlation with passive avoidance and water maze performance. *Neuroscience*, 53, 367–378.

Mikkonen, M., Alafuzoff, I., Tapiola, T., Soininen, H., & Miettinen, R. (1999). Subfield- and layer-specific changes in parvalbumin, calretinin and calbindin-D28K immunoreactivity in the entorhinal cortex in Alzheimer's disease. *Neuroscience*, 92, 515–532.

Mikkonen, M., Soininen, H., & Pitkänen, A. (1997). Distribution of parvalbumin-, calretinin-, and calbindin-D28k-immunoreactive neurons and fibers in the human entorhinal cortex. *Journal of Comparative Neurology*, 388, 64–88.

Morales, M., & Bloom, F. E. (1997). The 5-HT3 receptor is present in different subpopulations of GABAergic neurons in the rat telencephalon. *Journal of Neuroscience*, 17, 3157–3167.

Murray, H. C., Low, V. F., Swanson, M. E., Dieriks, B. V., Turner, C., Faull, R. L., & Curtis, M. A. (2016). Distribution of PSA-NCAM in normal, Alzheimer's and Parkinson's disease human brain. *Neuroscience*, 330, 359–375.

Murray, H. C., Swanson, M. E. V., Dieriks, B. V., Turner, C., Faull, R. L. M., & Curtis, M. A. (2018). Neurochemical characterization of PSA-NCAM(+) cells in the human brain and phenotypic quantification in Alzheimer's disease entorhinal cortex. *Neuroscience*, 372, 289–303.

Naumann, R. K., Ray, S., Prokop, S., Las, L., Heppner, F. L., & Brecht, M. (2016). Conserved size and periodicity of pyramidal patches in layer 2 of medial/caudal entorhinal cortex. *Journal of Comparative Neurology*, 524, 783–806.

Navarro Schroder, T., Haak, K. V., Zaragoza Jimenez, N. I., Beckmann, C. F., & Doeller, C. F. (2015). Functional topography of the human entorhinal cortex. *Elife*, *4*, e06738.

Nilssen, E. S., Jacobsen, B., Fjeld, G., Nair, R. R., Blankvoort, S., Kentros, C., & Witter, M. P. (2018). Inhibitory connectivity dominates the fan cell network in layer II of lateral entorhinal cortex. *Journal of Neuroscience*, 9712–9727.

Nyíri, G., Freund, T. F., & Somogyi, P. (2001). Input-dependent synaptic targeting of α2-subunit-containing GABAA receptors in synapses of hippocampal pyramidal cells of the rat. *European Journal of Neuroscience*, *13*, 428–442.

Ohara, S., Itou, K., Shiraishi, M., Gianatti, M., Sota, Y., Kabashima, S., … Iijima, T. (2016). *Efferent projections of the calbindin-positive entorhinal neurons in the rat: Connectional differences between the medial and lateral entorhinal cortex SFN, Abstract 84.13*.

Ohara, S., Onodera, M., Simonsen, O. W., Yoshino, R., Hioki, H., Iijima, T., … Witter, M. P. (2018). Intrinsic projections of layer Vb neurons to layers Va, III, and II in the lateral and medial entorhinal cortex of the rat. *Cell Reports*, *24*, 107–116.

Olsen, G. M., & Witter, M. P. (2016). Posterior parietal cortex of the rat: Architectural delineation and thalamic differentiation. *Journal of Comparative Neurology*, *524*, 3774–3809.

Pantazopoulos, H., Woo, T. U., Lim, M. P., Lange, N., & Berretta, S. (2010). Extracellular matrix-glial abnormalities in the amygdala and entorhinal cortex of subjects diagnosed with schizophrenia. *Archives of General Psychiatry*, *67*, 155–166.

Papp, E. C., Hajos, N., Acsady, L., & Freund, T. F. (1999). Medial septal and median raphe innervation of vasoactive intestinal polypeptide-containing interneurons in the hippocampus. *Neuroscience*, *90*, 369–382.

Pastoll, H., Solanka, L., van Rossum, M. C., & Nolan, M. F. (2013). Feedback inhibition enables theta-nested gamma oscillations and grid firing fields. *Neuron*, *77*, 141–154.

Paulussen, M., Jacobs, S., Van der Gucht, E., Hof, P. R., & Arckens, L. (2011). Cytoarchitecture of the mouse neocortex revealed by the low-molecular-weight neurofilament protein subunit. *Brain Structure and Function*, *216*, 183–199.

Pazos, A., Probst, A., & Palacios, J. M. (1987). Serotonin receptors in the human brain—III. Autoradiographic mapping of serotonin-1 receptors. *Neuroscience*, *21*, 97–122.

Perez-Garcia, C. G., Gonzalez-Delgado, F. J., Suarez-Sola, M. L., Castro-Fuentes, R., Martin-Trujillo, J. M., Ferres-Torres, R., & Meyer, G. (2001). Reelin-immunoreactive neurons in the adult vertebrate pallium. *Journal of Chemical Neuroanatomy*, *21*, 41–51.

Pesold, C., Impagnatiello, F., Pisu, M., Uzunov, D., Costa, E., Guidotti, A., & Caruncho, H. (1998). Reelin is preferentially expressed in neurons synthesizing γ-aminobutyric acid in cortex and hippocampus of adult rats. *Proceedings of the National Academy of Sciences*, *95*, 3221–3226.

Phan, A. (2015). *Immunohistochemical and morphological characterization of GABAergic cells in LEC*. Trondheim, Norway: Norwegian University of Science and Technology, Department of Neuroscience.

Pitkänen, A., & Amaral, D. G. (1993). Distribution of parvalbumin-immunoreactive cells and fibers in the monkey temporal lobe: The hippocampal formation. *Journal of Comparative Neurology*, *331*, 37–74.

Pothuizen, H. H., Feldon, J., & Jongen-Relo, A. L. (2004). Co-expression of calretinin and gamma-aminobutyric acid in neurons of the

entorhinal cortex of the common marmoset monkey. *Hippocampus*, *14*, 615–627.

Ramos-Moreno, T., Galazo, M. J., Porrero, C., Martinez-Cerdeno, V., & Clasca, F. (2006). Extracellular matrix molecules and synaptic plasticity: Immunomapping of intracellular and secreted Reelin in the adult rat brain. *European Journal of Neuroscience*, *23*, 401–422.

Ramsden, H. L., Surmeli, G., McDonagh, S. G., & Nolan, M. F. (2015). Laminar and dorsoventral molecular organization of the medial entorhinal cortex revealed by large-scale anatomical analysis of gene expression. *PLoS Computational Biology*, *11*, e1004032.

Ray, S., Naumann, R., Burgalossi, A., Tang, Q., Schmidt, H., & Brecht, M. (2014). Grid-layout and theta-modulation of layer 2 pyramidal neurons in medial entorhinal cortex. *Science*, *343*, 891–896.

Riedel, A., Miettinen, R., Stieler, J., Mikkonen, M., Alafuzoff, I., Soininen, H., & Arendt, T. (2003). Reelin-immunoreactive Cajal-Retzius cells: The entorhinal cortex in normal aging and Alzheimer's disease. *Acta Neuropathologica*, *106*, 291–302.

Rogers, J. H. (1992). Immunohistochemical markers in rat cortex: Co-localization of calretinin and calbindin-D28k with neuropeptides and GABA. *Brain Research*, *587*, 147–157.

Rosene, D. L., & Van Hoesen, G. W. (1987). The hippocampal formation of the primate brain. In E. G. Jones, & A. Peters (Eds.), *Cerebral cortex* (pp. 345–456). Boston, MA: Springer.

Rowland, D. C., Roudi, Y., Moser, M. B., & Moser, E. I. (2016). Ten years of grid cells. *Annual Review of Neuroscience*, *39*, 19–40.

Saiz-Sanchez, D., Ubeda-Banon, I., De la Rosa-Prieto, C., & Martinez-Marcos, A. (2012). Differential expression of interneuron populations and correlation with amyloid-β deposition in the olfactory cortex of an AβPP/PS1 transgenic mouse model of Alzheimer's disease. *Journal of Alzheimer's Disease*, *31*, 113–129.

Savasta, M., Palacios, J. M., & Mengod, G. (1990). Regional distribution of the messenger RNA coding for the neuropeptide cholecystokinin in the human brain examined by in situ hybridization. *Molecular Brain Research*, *7*, 91–104.

Schmidt, S., Braak, E., & Braak, H. (1993). Parvalbumin-immunoreactive structures of the adult human entorhinal and transentorhinal region. *Hippocampus*, *3*, 459–470.

Schwarcz, R., & Witter, M. P. (2002). Memory impairment in temporal lobe epilepsy: The role of entorhinal lesions. *Epilepsy Research*, *50*, 161–177.

Seeger, G., Brauer, K., Härtig, W., & Brückner, G. (1994). Mapping of perineuronal nets in the rat brain stained by colloidal iron hydroxide histochemistry and lectin cytochemistry. *Neuroscience*, *58*, 378–388.

Seress, L., Leranth, C., & Frotscher, M. (1994). Distribution of calbindin D28k immunoreactive cells and fibers in the monkey hippocampus, subicular complex and entorhinal cortex. A light and electron microscopic study. *Journal fur Hirnforschung*, *35*, 473–486.

Seress, L., Nitsch, R., & Leranth, C. (1993). Calretinin immunoreactivity in the monkey hippocampal formation-I. Light and electron microscopic characteristics and co-localization with other calcium-binding proteins. *Neuroscience*, *55*, 775–796.

Sijbesma, H., Schipper, J., Cornelissen, J. C. H. M., & Dekloet, E. R. (1991). Species-differences in the distribution of central 5-Ht1 binding-sites – A comparative autoradiographic study between rat and guinea-pig. *Brain Research*, *555*, 295–304.

Silberberg, G., & Markram, H. (2007). Disynaptic inhibition between neocortical pyramidal cells mediated by Martinotti cells. *Neuron*, *53*, 735–746.

Smaluhn, N., Plaschke, M., Leranth, C., & Nitsch, R. (2000). The transentorhinal cortex of the African green monkey: A combined light- and electron-microscopic study of calcium-binding protein containing neurons. *Anatomy and Embryology (Berlin)*, *202*, 143–158.

Sobreviela, T., & Mufson, E. J. (1995). Reduced nicotinamide adenine dinucleotide phosphate-diaphorase/nitric oxide synthase profiles in the human hippocampal formation and perirhinal cortex. *Journal of Comparative Neurology*, *358*, 440–464.

Solodkin, A., Veldhuizen, S. D., & Van Hoesen, G. W. (1996). Contingent vulnerability of entorhinal parvalbumin-containing neurons in Alzheimer's disease. *Journal of Neuroscience*, *16*, 3311–3321.

Somogyi, J., Baude, A., Omori, Y., Shimizu, H., Mestikawy, S. E., Fukaya, M., … Somogyi, P. (2004). GABAergic basket cells expressing cholecystokinin contain vesicular glutamate transporter type 3 (VGLUT3) in their synaptic terminals in hippocampus and isocortex of the rat. *European Journal of Neuroscience*, *19*, 552–569.

Stensola, H., Stensola, T., Solstad, T., Froland, K., Moser, M. B., & Moser, E. I. (2012). The entorhinal grid map is discretized. *Nature*, *492*, 72–78.

Stephan, H. (1975). *Handbuch der mikroskopischen Anatomie des Menschen*. Berlin, Germany: Springer.

Surmeli, G., Marcu, D. C., McClure, C., Garden, D. L., Pastoll, H., & Nolan, M. F. (2015). Molecularly defined circuitry reveals input-output segregation in deep layers of the medial entorhinal cortex. *Neuron*, *88*, 1040–1053.

Suzuki, W. A., & Porteros, A. (2002). Distribution of calbindin D-28k in the entorhinal, perirhinal, and parahippocampal cortices of the macaque monkey. *Journal of Comparative Neurology*, *451*, 392–412.

Swanson, L. W., Köhler, C., & Björklund, A. (1987). The limbic region. I. The septohippocampal system. In A. Björklund, T. Hökfelt, & L. W. Swanson (Eds.), *Handboook of chemical neuroanatomy* (Vol. 5, part 1, pp. 125–227). Amsterdam, the Netherlands: Elsevier Publisher.

Tahvildari, B., Wolfel, M., Duque, A., & McCormick, D. A. (2012). Selective functional interactions between excitatory and inhibitory cortical neurons and differential contribution to persistent activity of the slow oscillation. *Journal of Neuroscience*, *32*, 12165–12179.

Tamamaki, N., & Nojyo, Y. (1993). Projection of the entorhinal layer II neurons in the rat as revealed by intracellular pressure-injection of neurobiotin. *Hippocampus*, *3*, 471–480.

Thorns, V., Licastro, F., & Masliah, E. (2001). Locally reduced levels of acidic FGF lead to decreased expression of 28-kda calbindin and contribute to the selective vulnerability of the neurons in the entorhinal cortex in Alzheimer's disease. *Neuropathology*, *21*, 203–211.

Tsao, A., Moser, M. B., & Moser, E. I. (2013). Traces of experience in the lateral entorhinal cortex. *Current Biology*, *23*, 399–405.

Tsao, A., Sugar, J., Lu, L., Wang, C., Knierim, J. J., Moser, M. B., & Moser, E. I. (2018). Integrating time from experience in the lateral entorhinal cortex. *Nature*, *561*, 57–62.

Tuñón, T., Insausti, R., Ferrer, I., Sobreviela, T., & Soriano, E. (1992). Parvalbumin and calbindin D-28K in the human entorhinal cortex. An immunohistochemical study. *Brain Research*, *589*, 24–32.

Ueno, H., Fujii, K., Suemitsu, S., Murakami, S., Kitamura, N., Wani, K., … Takao, K. (2018). Expression of aggrecan components in perineuronal nets in the mouse cerebral cortex. *IBRO Reports*, *4*, 22–37.

Uva, L., Gruschke, S., Biella, G., De Curtis, M., & Witter, M. P. (2004). Cytoarchitectonic characterization of the parahippocampal region of the guinea pig. *Journal of Comparative Neurology*, *474*, 289–303.

Van Groen, T., Van Haren, F. J., Witter, M. P., & Groenewegen, H. J. (1986). The organization of the reciprocal connections between the subiculum and the entorhinal cortex in the cat: I. A neuroanatomical tracing study. *Journal of Comparative Neurology*, *250*, 485–497.

Varea, E., Belles, M., Vidueira, S., Blasco-Ibanez, J. M., Crespo, C., Pastor, A. M., & Nacher, J. (2011). PSA-NCAM is expressed in immature, but not recently generated, neurons in the adult cat cerebral cortex layer II. *Frontiers in Neuroscience*, *5*, 17.

Varea, E., Castillo-Gomez, E., Gomez-Climent, M. A., Blasco-Ibanez, J. M., Crespo, C., Martinez-Guijarro, F. J., & Nacher, J. (2007). PSA-NCAM expression in the human prefrontal cortex. *Journal of Chemical Neuroanatomy*, *33*, 202–209.

Varga, C., Lee, S. Y., & Soltesz, I. (2010). Target-selective GABAergic control of entorhinal cortex output. *Nature Neuroscience*, *13*, 822–824.

Wang, Y., Toledo-Rodriguez, M., Gupta, A., Wu, C., Silberberg, G., Luo, J., & Markram, H. (2004). Anatomical, physiological and molecular properties of Martinotti cells in the somatosensory cortex of the juvenile rat. *Journal of Physiology*, *561*, 65–90.

Witter, M. P. (2007). The perforant path: projections from the entorhinal cortex to the dentate gyrus. *Progress in Brain Research*, *163*, 43–61.

Witter, M. P. (2012). Hippocampus. In C. Watson, G. Paxinos, & L. Puelles (Eds.), *The mouse nervous system* (pp. 112–139). London, UK: Academic Press.

Witter, M. P., & Amaral, D. G. (1991). Entorhinal cortex of the monkey: V. Projections to the dentate gyrus, hippocampus, and subicular complex. *Journal of Comparative Neurology*, *307*, 437–459.

Witter, M. P., Doan, T. P., Jacobsen, B., Nilssen, E. S., & Ohara, S. (2017). Architecture of the entorhinal cortex a review of entorhinal anatomy in rodents with some comparative notes. *Frontiers in Systems Neuroscience*, *11*, 46.

Witter, M. P., & Groenewegen, H. J. (1984). Laminar origin and septo-temporal distribution of entorhinal and perirhinal projections to the hippocampus in the cat. *Journal of Comparative Neurology*, *224*, 371–385.

Wolansky, T., Pagliardini, S., Greer, J. J., & Dickson, C. T. (2007). Immunohistochemical characterization of substance P receptor (NK(1)R)-expressing interneurons in the entorhinal cortex. *Journal of Comparative Neurology*, *3*, 427–441.

Wouterlood, F. G., Canto, C. B., Aliane, V., Boekel, A. J., Grosche, J., Härtig, W., … Witter, M. P. (2007). Coexpression of vesicular glutamate transporters 1 and 2, glutamic acid decarboxylase and calretinin in rat entorhinal cortex. *Brain Structure and Function*, *212*, 303–319.

Wouterlood, F. G., & Härtig, W. (1995). Calretinin-immunoreactivity in mitral cells of the rat olfactory bulb. *Brain Research*, *682*, 93–100.

Wouterlood, F. G., Härtig, W., Brückner, G., & Witter, M. P. (1995). Parvalbumin-immunoreactive neurons in the entorhinal cortex of the rat: Localization, morphology, connectivity and ultrastructure. *Journal of Neurocytology*, *24*, 135–153.

Wouterlood, F. G., & Pothuizen, H. (2000). Sparse colocalization of somatostatin- and GABA-immunoreactivity in the entorhinal cortex of the rat. *Hippocampus*, *10*, 77–86.

Wouterlood, F. G., van Denderen, J. C., van Haeften, T., & Witter, M. P. (2000). Calretinin in the entorhinal cortex of the rat: Distribution, morphology, ultrastructure of neurons, and co-localization with gamma-aminobutyric acid and parvalbumin. *Journal of Comparative Neurology*, *425*, 177–192.

Wyss, M. J. (1981). An autoradiographic study of the efferent connections of the entorhinal cortex in the rat. *Journal of Comparative Neurology*, *199*, 495–512.

Ye, J., Witter, M. P., Moser, M. B., & Moser, E. I. (2018). Entorhinal fast-spiking speed cells project to the hippocampus. *Proceedings of the National Academy of Sciences of the United States of America*, *115*, E1627–E1636.

Yew, D. T., Wong, H. W., Li, W. P., Lai, H. W., & Yu, W. H. (1999). Nitric oxide synthase neurons in different areas of normal aged and Alzheimer's brains. *Neuroscience*, *89*, 675–686.

Zeineh, M. M., Palomero-Gallagher, N., Axer, M., Grassel, D., Goubran, M., Wree, A., … Zilles, K. (2017). Direct visualization and mapping of the spatial course of fiber tracts at microscopic resolution in the human hippocampus. *Cerebral Cortex*, *27*, 1779–1794.

SUPPORTING INFORMATION

Additional supporting information may be found online in the Supporting Information section at the end of the article.

How to cite this article: Kobro-Flatmoen A, Witter MP. Neuronal chemo-architecture of the entorhinal cortex: A comparative review. *Eur J Neurosci.* 2019;50:3627–3662. https://doi.org/10.1111/ejn.14511